



# Oxygen Level and Particle Size Effects on Sintering of Binder Jetting Copper Parts

Master Thesis

In Department of Material Science and Engineering

by

Cem Özateş

ORCID 0000-0001-6949-7818

June, 2022

This is to certify that we have read the thesis **Oxygen Level and Particle Size Effects on Sintering of Binder Jetting Copper Parts** submitted by **Cem Özateş**, and it has been judged to be successful, in scope and in quality, at the defense exam and accepted by our jury as a MASTER'S THESIS.

**APPROVED BY:**

**Advisor:**

**Assoc. Prof. Onur Ertuğrul**  
İzmir Kâtip Çelebi University

**Committee Members:**

**Assoc. Prof. Onur Ertuğrul**  
İzmir Kâtip Çelebi University

**Assoc. Prof. Uğur Çavdar**  
İzmir Demokrasi University

**Assist. Prof. Bahadır Uyulgan**  
Dokuz Eylül University

**Date of Defense: July 29, 2022**

# Declaration of Authorship

I, **Cem Özateş**, declare that this thesis titled **Oxygen Level and Particle Size Effects on Sintering of Binder Jetting Copper Parts** and the work presented in it are my own. I confirm that:

- This work was done wholly or mainly while in candidature for the Master's degree at this university.
- Where any part of this thesis has previously been submitted for a degree or any other qualification at this university or any other institution, this has been clearly stated.
- Where I have consulted the published work of others, this is always clearly attributed.
- Where I have quoted from the work of others, the source is always given. This thesis is entirely my own work, with the exception of such quotations.
- I have acknowledged all major sources of assistance.
- Where the thesis is based on work done by myself jointly with others, I have made clear exactly what was done by others and what I have contributed myself.

Date: 29.07.2022

---

# Oxygen Level and Particle Size Effects on Sintering of Binder Jetting Copper Parts

## Abstract

Copper is one of the most conductive metallic materials. For most metals, additive manufacturing is prone to laser or electron beam powder bed fusion processes. Due to copper's high reflectivity and very high thermal conductivity, it is difficult to print 3D parts with powder bed fusion methods. Binder jetting, which is a developing 3D printing technology, has a high potential for use in order to eliminate these problems of copper and low processing costs. In this study, the effect of particle size distribution and oxygen level of the copper powders on part density, tensile strength, surface roughness and electrical properties of the final parts were investigated. After the sintering parameters study, it is seen that 1070°C and 100% H<sub>2</sub> are required for sintering temperature and atmosphere. When we compare L-O 10-63 to L-O15-45, it was observed that the surface porosity was very low but the internal porosity was high and larger in the samples with L-O 10-63. In H-O 15-45 samples, there is an inhomogeneity for the pore distribution along the cross section. Also, the best results of tensile tests and electrical conductivity are obtained with low oxygen content of 15–45 μm particle size copper powders. The powder with high oxygen level resulted in lower results than the powder with low oxygen.

**Keywords:** Additive manufacturing, binder jetting, copper, particle size, oxygen level

# Bağlayıcı Püskürtmeli Eklemeli İmalat Yönteminde Bakır Parçaların Sinterlenmesinde Tane Boyutunun ve Oksijen Seviyesinin Etkisi

## ÖZ

Bakır en iletken metalik malzemelerden biridir. Çoğu metal için, eklemeli imalat, lazer veya elektron ışını toz yatağı füzyon işlemlerine eğilimlidir. Bakırın yüksek yansıtma özelliği ve çok yüksek ısı iletkenliği nedeniyle toz yatak füzyon yöntemleriyle 3 boyutlu parçaların basılması zordur. Bağlayıcı püskürtmeli eklemeli imalat yöntemi ile bakırın bu problemlerini ortadan kaldırmak için kullanım potansiyeli yüksek olup, düşük işleme maliyetleri gibi avantajları ile öne çıkmaktadır. Bu çalışmada, bakır tozlarının partikül boyutu dağılımının ve oksijen seviyesinin, nihai parçaların parça yoğunluğu, çekme mukavemeti, yüzey pürüzlülüğü ve elektriksel özellikleri üzerindeki etkisi araştırılmıştır. Sinterleme parametreleri çalışmasından sonra, sinterleme sıcaklığı ve atmosferi için 1070°C ve %100 H<sub>2</sub> gerekli olduğu görülmüştür. Düşük oksijenli 10-63 ile 15-45'i karşılaştırdığımızda, Düşük oksijenli 10-63 ile numunelerde yüzey gözenekliliğinin çok düşük olduğu ancak iç gözenekliliğin yüksek ve daha büyük olduğu gözlemlendi. Yüksek oksijenli 15-45 numunelerinde ise enine kesit boyunca gözenek dağılımı için bir homojenlik yoktur.. Öte yandan çekme testi ve elektriksel iletkenlik açısından en iyi sonuçlar, düşük oksijen içeriği 15-45 µm partikül boyutunda bakır tozları ile elde edilmektedir. Oksijen seviyesi yüksek olan tozlar, düşük oksijenli tozlardan daha düşük sonuçlar göstermiştir.

**Anahtar Kelimeler:** Eklemeli imalat, bağlayıcı püskürtmeli eklemeli imalat yöntemi, bakır, tane dağılımı, oksijen seviyesi

*To my Family*

# Acknowledgment

I would like to express my deep and very great appreciation to my Assoc. Prof. Dr. Onur Ertuğrul for his valuable supports and constructive suggestions during this research work. I would also like to thank Assoc. Prof. Dr. Emrecaan Soylemez for sharing his advices and supports. I am also grateful to Sentes-BIR AS Managing Director Cagrı Gurbuz, Sentes-BIR R&D Center Director Esm a Ercengiz, and my colleagues B ulent Gen and Beyza Bilgiler who helped me with pleasure during my thesis.

# Table of Contents

Declaration of Authorship	ii
Abstract	iii
Öz	iv
Acknowledgment	vi
List of Figures	x
List of Tables	xiii
List of Abbreviations	xiv
List of Symbols	xv
<b>1 Introduction</b>	<b>1</b>
1.1 Aim and Objective of the Thesis	1
1.2 Theoretical Background	2
1.2.1 Additive Manufacturing	2
1.2.2 Additive Manufacturing Techniques	3
1.2.2.1 Directed Energy Deposition	3
1.2.2.2 Powder Bed Fusion	4
1.2.2.2.1 Selective Laser Sintering/melting	5
1.2.2.2.2 Selective Electron Beam Melting	6
1.2.2.3 Sheet Lamination	8
1.2.2.4 Material Extrusion	9
1.2.2.5 Material Jetting	9
1.2.2.6 Vat Photo Polymerization	10
1.2.2.7 Binder Jetting	11

1.2.2.7.1	The Advantages of Binder Jetting	13
1.2.2.7.2	The Disadvantages of Binder Jetting	14
1.2.3	Binder Jetting Parameters	14
1.2.3.1	Powder Production Methods	15
1.2.4	Binder Jetting Materials	19
1.2.5	Copper in Binder Jetting Technology	20
1.3	Literature Review	23
<b>2</b>	<b>Materials and Methods</b>	<b>26</b>
2.1	Experimental Studies	26
2.2	Powder Preparation	26
2.2.1	Sieving	26
2.2.2	Air Classifier	27
2.3	Powder Characterization	28
2.3.1	Helium Pycnometry	28
2.3.2	Particle Size Analyzer	29
2.3.3	Apparent Density and Flow Measurement	30
2.3.4	Tap Density Measurement	30
2.3.5	Elemental Analyzer	31
2.3.6	SEM Analyses	32
2.4	Binder Jetting Production Procedure	33
2.4.1	3D Cad Model	33
2.4.2	Layer Thickness and Binder Saturation	35
2.5	Effect of Sintering Atmosphere and Temperature	36
2.6	Characterization Techniques	38
2.6.1	Density, Porosity and Shrinkage of Samples	38
2.6.2	Microstructure Characterization	38
2.6.3	Surface Roughness	40

2.6.4	Tensile Tests	40
2.6.5	Electrical Conductivity Tests	41
<b>3</b>	<b>Results and Discussion</b>	<b>43</b>
3.1	Benchtop Test Results	43
3.1.1	Importance of Binder Ratio	43
3.1.2	Curing Behavior	44
3.2	Powder Characterization Results	46
3.3	Sintering Parameter Optimization Results	49
3.3.1	Effects of Sintering Temperature on Density	49
3.3.2	Effects of Binder Ratio on Density	52
3.3.3	Effects of Sintering Atmosphere on Density	52
3.3.4	Effects of Sintering Time on Density	53
3.3.5	Effects of Reduction Process Temperature on Density	53
3.4	Density, Porosity and Shrinkage Results	54
3.5	Optical Microscopy	56
3.6	Surface Roughness Measurements	59
3.7	Electrical Properties	59
3.8	Tensile Tests Results	60
<b>4</b>	<b>Conclusions</b>	<b>63</b>
	<b>References</b>	<b>65</b>
	<b>Appendices</b>	<b>72</b>
Appendix A	Publications from the Thesis	73
Appendix B	Front Cover	74
	<b>Curriculum Vitae</b>	<b>77</b>

# List of Figures

Figure 1.1 Additive manufacturing (3D printing) process step	2
Figure 1.2 Types of directed energy deposition	4
Figure 1.3 Schematic of typical SLM machine	6
Figure 1.4 EBM process chamber	7
Figure 1.5 Sheet lamination process	8
Figure 1.6 Material Extrusion process	9
Figure 1.7 Material Jetting process	10
Figure 1.8 A sample SLA (Stereolithography) device	10
Figure 1.9 Schematic of the BJT process	11
Figure 1.10 A tube furnace for sintering	12
Figure 1.11 Schematic diagram of gas atomization processing	16
Figure 1.12 Scanning electron micrographs of atomized powders. (a) water atomized iron powder; (b) gas atomized high carbon steel; (c) centrifugally atomized nickel-base superalloy (plasma rotating electrode process); (d) vacuum atomized nickel-base superalloy	17
Figure 1.13 Changing mechanism of packing density of spherical and irregular ceramic powders after powder spreading	18
Figure 1.14 Scientific document amount related to binder jetting metal additive manufacturing reported in the literature	20
Figure 1.15 A DM Cu 3D printed a heat sink gyroid	21
Figure 1.16 The damage to the optical mirror	22
Figure 1.17 Complex-shaped copper made via binder jetting	23
Figure 2.1 An ultrasonic sieve	27
Figure 2.2 An illustration of air classifier 1. Feeding system, 2. Air Classifier-1, 3. Air Classifier-2, 4. Air Classifier-3, 5. Cyclone collector, 6. Dust collector, 7. Draught fan, 8. Electrical control system	27
Figure 2.3 Micromeritics AccuPyc II 1340 helium pycnometer	29

Figure 2.4	Malvern Hydro 2000	29
Figure 2.5	The standard schematic of flowmeter apparatus — Hall Funnel	30
Figure 2.6	Example of Tapping Apparatus	31
Figure 2.7	(a) Eltra Carbon/Sulphur analyzer, (b) Leco oxygen/nitrogen analyzer	32
Figure 2.8	Scanning electron microscope (SEM)	32
Figure 2.9	Design of tensile stress sample (ASTM E8/E8M-16a)	34
Figure 2.10	Cube samples produced with binder jetting	36
Figure 2.11	Sintering Regime	37
Figure 2.12	Protherm tubular furnace	37
Figure 2.13	(a) acrylic cold mounting, (b) hardener, and (c) mould	38
Figure 2.14	Automatic grinding & polishing machine	39
Figure 2.15	Nikon Eclipse Optical Microscope	39
Figure 2.16	Linear Profilometer	40
Figure 2.17	Shimadzu Tensile test machine	41
Figure 2.18	4-point measurements apparatus	42
Figure 3.1	(a) Cured sample in the bar (200 °C for 2 hours), (b) Cured sample in pieces	44
Figure 3.2	(a) Cured part in steel bar (b) cured bar in carbon bar (c) cured part in fiber bar	44
Figure 3.3	(a) Silicon bars, (b) Cured bars at 200 °C for 2 hours	45
Figure 3.4	(a) Benchtop test samples before curing, (b) Benchtop test samples after curing in argon atmosphere	45
Figure 3.5	(a) Particle size distributions of 15-45 µm low oxygen, (b) 15-45 µm high oxygen, c) 10-63 µm low oxygen copper powders	48
Figure 3.6	SEM images of lower and higher magnifications of (a,b) 15-45 µm low oxygen powders, (c,d) 15-45 µm high oxygen powders, and (e,f) 10-63 µm low oxygen powders	49
Figure 3.7	Effect of sintering atmosphere on the density of parts with 15-45 µm powders. Sample 1 & 2 sintered with 95/5% N <sub>2</sub> /H <sub>2</sub> and sample 3 & 4 sintered with 100% H <sub>2</sub>	53
Figure 3.8	Effects of sintering atmosphere. Sample 1 & 2 sintered at 1070 °C 2 hours and Sample 3 & 4 sintered at 1070 °C 4 hours	53

Figure 3.9 Effects of sintering atmosphere. Sample 1 & 2 sintered at 1070 °C 2 hours and Sample 3 & 4 sintered at 1070 °C 4 hours	53
Figure 3.10 (a) High oxygen content 15-45 μm green parts printed with binder jetting, (b) sintered LO-10-63 cubes, and (c) sintered LO-15-45 parts	55
Figure 3.11 Optical microscope images of (a,b,c,d) LO-15-45, (e,f,g,h) HO-15-45, and (i,j,k,l) LO-10-63 parts	58
Figure 3.12 (a) High oxygen content 15-45 μm green parts printed with binder jetting, (b) sintered LO-10-63 cubes, and (c) sintered LO-15-45 parts	58

# List of Tables

Table 1.1	The advantages and disadvantages of binder jetting	13
Table 1.2	Important parameters of binder jetting	15
Table 2.1	Representative sample coding	28
Table 2.2	Diameter of characterization samples	34
Table 2.3	Diameter of tensile test samples	35
Table 3.1	Powder and binder ratios for benchtop test mixtures	43
Table 3.2	Powder characterization results of the all copper powders. The results were added by averaging as a result of five consistent measurements	49
Table 3.3	Comparison of benchtop test and binder jetting samples at 1040 °C for 130 min. under 5% hydrogen and 95% nitrogen atmosphere	50
Table 3.4	Comparison of benchtop test and binder jetting samples at 1050 °C for 130 min. in 95/5% nitrogen/hydrogen atmosphere	51
Table 3.5	Comparison of benchtop test and binder jetting samples at 1070 °C for 130 min. in 95/5% nitrogen/hydrogen atmosphere	51
Table 3.6	Sintering results of samples that printed with the parameter of low binder/85 µm layer thickness and middle binder/120 µm thickness	52
Table 3.7	Comparison of green, sintered and relative density, porosity and shrinkage results. The results were added by averaging the five consistent measurements	56
Table 3.8	Comparison of surface roughness	59
Table 3.9	Electrical conductivity test results	60
Table 3.10	Tensile test results	61

# List of Abbreviations

L-O-14-45	Low oxygen content 15-45 $\mu\text{m}$ copper powder
H-O-14-45	High oxygen content 15-45 $\mu\text{m}$ copper powder
L-O-10-63	Low oxygen content 10-63 $\mu\text{m}$ copper powder
Cu	Copper
ORCID	Open Researcher and Contributor ID
SLS/SLM	Selective laser sintering/melting
EBM	Electron Beam Melting
AM	Additive Manufacturing
3D	3 Dimension
ASTM	American Society for Testing and Materials
FDM	Fused Deposition Modelling
PBF	Powder Bed Fusion
LBM	Laser Beam Melting
DMLS	Direct Metal Laser Sintering
BJT	Binder Jetting Technology
ABS	Acrylonitrile Butadiene Styrene
PVA	Polyvinyl Alcohol
PP	Polypropylene
MJ	Material Jetting
SLA	Stereolithography
DLP	Digital Light Processing
MIT	Massachusetts Institute of Technology

## List of Symbols

$H_2$	Hydrogen
$\mu m$	Micron
$N_2$	Nitrogen
ppm	Parts Per Million
Cu	Copper

# Chapter 1

## Introduction

### 1.1 Aim and Objective of the Thesis

Additive manufacturing (AM) is a process of joining metal powders layer by layer in order to make complex shaped objects using 3D model data. The use of Additive Manufacturing (AM) with metal powders is a new and growing industrial sector. Additive Manufacturing is different from traditional manufacturing methods in which materials are produced, then reshaped, machined, or otherwise finished. Titanium, steel, stainless steel, aluminum and copper, cobalt chrome, titanium and nickel-based alloy powders are used in additive manufacturing. [1]

Copper is one of the most conductive metallic materials. Its electrical and thermal conductivity is second only to silver. For most metals, 3D printing is mostly done by laser or electron beam powder bed fusion processes. [2] Due to copper's high reflectivity and very good thermal and electrical conductivity, it becomes very difficult to print 3D parts with powder bed fusion methods. Also, both methods are very costly additive manufacturing methods for producing 3D copper parts. Binder jetting additive manufacturing method, which is nearly a new 3D printing technology has a high potential for use in order to eliminate these problems of copper and stands out with its advantages such as multiple part production and low processing costs. The aim of this thesis study is to investigate the effects of the powder size distribution and the oxygen amount in copper powders on the density, mechanical, electrical properties of the final part which is produced by Binder Jetting technology. Sintering parameters optimization and binder jetting parameters optimizations have been carried out and their results have been also discussed.

## 1.2 Theoretical Background

### 1.2.1 Additive Manufacturing

Additive manufacturing (AM) enables the production of parts that are difficult and/or impossible to produce with traditional methods. The most important advantages are; the use of a wide variety of materials such as polymers, metals and composites, flexibility in design, the ability to combine 3D model data and materials layer by layer to produce complex shaped parts with very precise dimensional accuracy. In addition, complex geometries such as honeycomb structure and cooling channels can also be produced easily. It has also advantages that enables lightening, extends product life and reduce material waste. [3]

Since additive manufacturing has a high manufacturability potential compared to traditional methods, it provides an advantage in producing optimized complex designs. Resins and thermoplastic polymers, metals such as titanium and superalloys, and composites are the most used materials in additive manufacturing.[4]

The use of Additive Manufacturing (AM) with metal powders is a new and growing industry sector. Additive Manufacturing is different from traditional manufacturing methods in which materials are produced, then reshaped, machined, or otherwise finished. Titanium, steel, stainless steel, aluminum and copper, cobalt chrome, titanium and nickel-based alloy powders are used in additive manufacturing. [5]

The part designed in the computer environment, as shown in Figure 1.1, is converted into the required format (\*.STL) and divided into layers, and additive manufacturing machines create these layers according to their unique technique.[6]



Figure 1.1: Additive manufacturing (3D printing) process step

## 1.2.2 Additive Manufacturing Techniques

According to ISO/ASTM standards (ASTM F2792), the techniques used to create additive manufacturing layers fall into seven categories, the first four on the list being suitable for metals.

- Directed Energy Deposition
- Powder Bed Fusion
- Sheet Lamination
- Material Extrusion
- Material Jetting
- Vat Photo Polymerization
- Binder jetting

### 1.2.2.1 Directed Energy Deposition

The directed energy deposition process is based on a raw material feeder and energy source as shown in Figure 1.2, melting the material and depositing the molten material on the sheet. Although it is similar to classical FDM systems in that it forms the part by stacking the molten material in layers, it has great differences in terms of both raw material and energy source.

Although it is mostly used in industrial applications such as repairing damaged turbine blades and propellers, it is also possible to manufacture parts from scratch with this method. Compared to other metal additive manufacturing applications (SLM, SLS), more efficient and larger parts can be produced. However, it is impossible to produce complex geometries such as lattice structures with this method. This method is preferred for coarser geometries where high resolution is not required.[7]

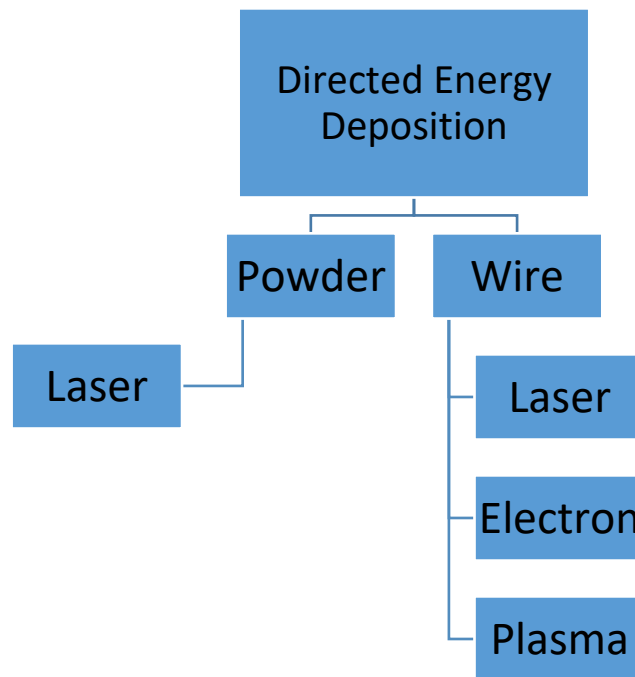


Figure 1.2: Types of directed energy deposition

#### Wire & powder system comparison

- Wire fed systems are more economical due to the low cost of raw materials
- The deposition rate per unit time is higher in wire systems.
- The surface roughness of the final product is much higher in wire fed system.

Therefore, the post-process requirement is more.

Directed energy deposition method has advantages such as high accumulation rate, rapid prototyping, lower raw material cost compared to powder bed laser systems, large-size parts production, high-strength parts production, repair of damaged parts with this method, its use in processes such as adding external coating to existing parts, and efficient raw material use. In addition, it has disadvantages such as the high initial investment cost compared to other methods and the high surface roughness, especially in wire-fed systems.[8]

#### 1.2.2.2 Powder Bed Fusion

Powder bed fusion technologies are based on the principle of fusing powdered materials by melting or heating, using a power source such as laser, infrared light

source and electron beam. In this method, powder materials are spread on a building table in layers. Each layer is processed in a controlled manner by melting only required areas with a laser. These processes continue one after the other, eventually forming the part.[9]

During part production, various parameters affect part quality. These depend on the parameters of the machine used, material properties, manufacturing environment conditions and part design. Machine parameters; layer thickness, scanning speed, scanning distance, laser focus diameter, laser power, scanning strategy, etc. can be listed as Material properties can be any physical and chemical properties of the material. The manufacturing environment includes factors such as temperature and atmosphere. Part design, on the other hand, covers various parameters such as the geometry of the part and its positioning on the table. [10]

PBF is classified into laser beam melting (LBM), electron beam melting (EBM), and selective laser sintering/melting (SLS/SLM). Binder Jetting technology is also a powder bed based additive manufacturing method; however, binder is used instead of using power source to fusion powders. Therefore, it is usually classified in sinter based additive manufacturing. [11]

#### 1.2.2.2.1 Selective Laser Sintering/melting

Selective laser sintering/melting (SLS/SLM) is an additive manufacturing technique. The product, which is designed in 3D in the computer environment, is created in layers, mapped and these layers are produced layer by layer and take their final form. The 3D machine that will make the production must have a mechanism that can spread the material in powder form in layers of the desired thickness and an optical mechanism that can apply laser to the desired points. The dimensions of the products whose production is completed with SLM are very close to the designed dimensions. However, final operations may be required. [12]

In SLM technique, chipping is not necessary after production. Stress relieving, sand blasting and electrochemical polishing operations may be required. Stress relieving can be done after production in order to remove the thermal stresses that occur because laser is not applied to every point of the product at the same time. Apart from these,

since the product takes its final shape directly, it is superior to casting and tooling production techniques. [13]

During SLM production, one layer of powder material is spread at a time. As it can be seen in the Figure 1.3, the piston under the chamber where the raw material is stored rises each time by the layer thickness, while the piston in the product chamber decreases as the layer thickness. With the help of a roller, the new layer is layered the production chamber. The beam received from the laser source is with the help of mirrors that can scan all the coordinates in the production chamber and it is dropped on the new layer formed. The powder material on the parts where laser is not applied can be reused. [14]

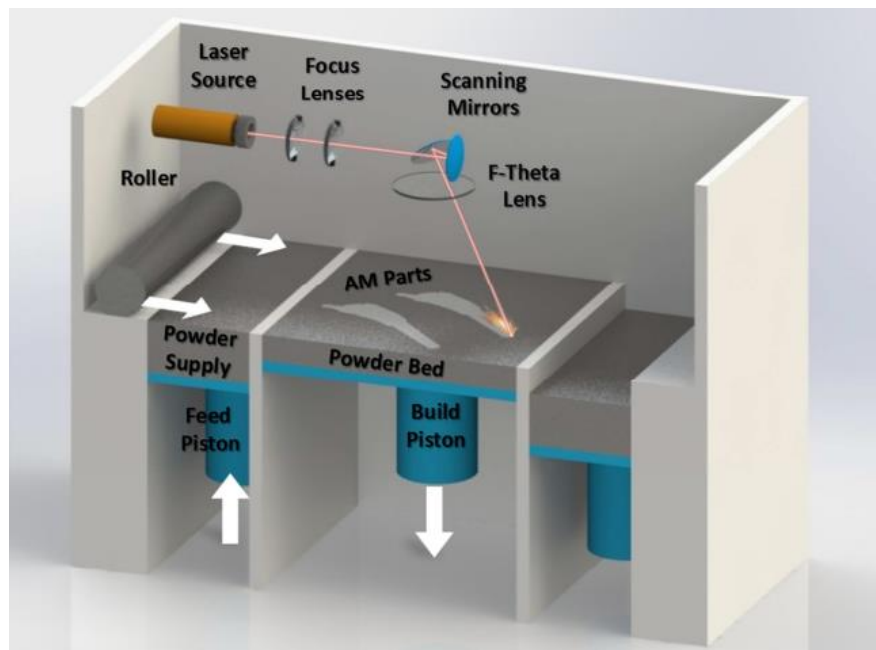


Figure 1.3: Schematic of typical SLM machine [15]

#### 1.2.2.2.2 Electron Beam Melting

Electron Beam Melting (EBM) is a powder bed fusion (PBF) method similar to (DMLS as a solid pattern is built from metal powders. The key difference is that in EBM the heat source is electron beams. EBM technology is a process that builds layer

by layer by melting completely dense metal powders with a powerful electron beam.  
[16]

The operation of the system begins with the sending of an electron beam from the filament as shown in Figure 1.4. A series of coils is used to control and scan the bundles. By accelerating the electrons between the cathode and the anode, the energy required for the melting of the powders is produced. The electron gun and the powder bed are in a vacuum system, thus providing an extremely clean and contamination-free environment.[17]

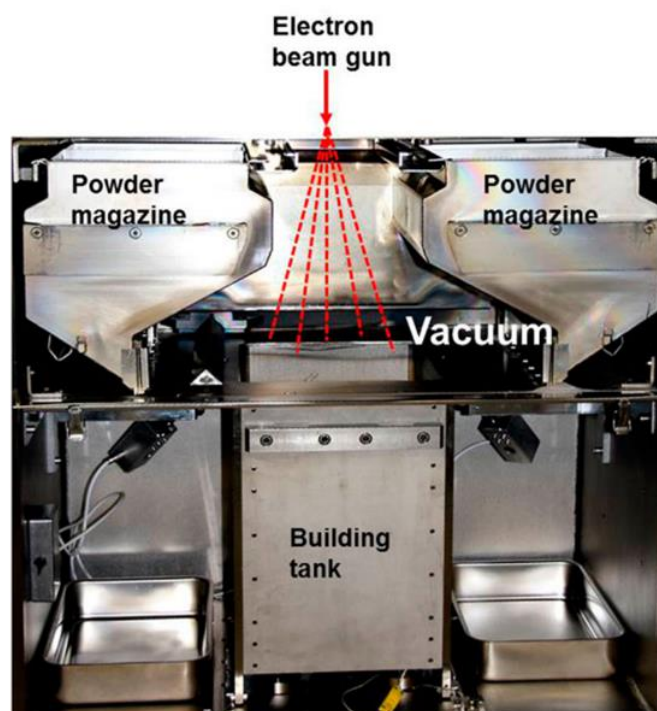


Figure 1.4: EBM process chamber [18]

The biggest difference between the EBM and SLS/SLM is in the preheating and the cooling process. While EBM Technology produces with preheating between 650 and 1100 degrees, DMLS/SLM/SLS systems produce at an ambient temperature of approximately 200 °C. Another important difference between the technologies is that laser-based systems operate under a gas atmosphere, while EBM systems operate under vacuum. [19]

In the EBM method, there is no need support structure to mechanically connect the parts to the table, as the parts are not mechanically stressed. This gives two main advantages; the first is that usage of short supports that are not mechanically attached to the table, instead of dense supports that are attached to the table, and the other one can use the production area to the end in the z direction by stacking them on top of each other. [[19,20]

The most well-known difference between EBM and DMLS systems is the differences in surface roughness and geometric tolerance. This difference is seriously dependent on the geometry, but the surface of the production of the laser system is cleaner and the geometric tolerance is more successful. [21]

### 1.2.2.3 Sheet lamination

During the sheet lamination process, sheets of adhesive-coated paper, plastic, or metal laminate are joined together using heat and pressure, and then shaped with a computer-controlled laser or knife as illustrated in Figure 1.5. Post-processing of 3D-printed parts includes steps such as machining and drilling.[22]

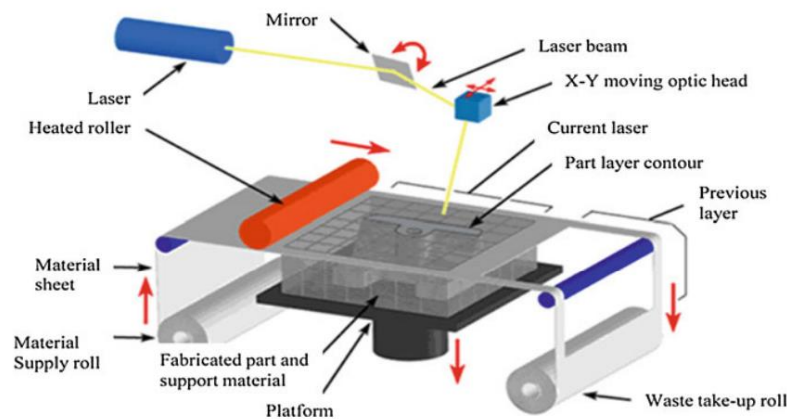


Figure 1.5: Sheet lamination process [23]

The work piece is positioned on the table. The activity of the adhesive is provided by heated rollers. The laser sent from the plotter type source; the cutting process is performed as desired according to the material thickness. When the process is completed, the system is cleaned of excess and support material. [24]

### 1.2.2.4 Material Extrusion

Material extrusion devices are the most common and cheapest 3D printers in the world. Material extrusion also called fused deposition modeling or FDM. Polymer materials consisting of PLA, ABS, Nylon, ASA, PETG, HIPS, FLEX, PCBS, PVA, and PP can produce models with desired chemical properties.[25]

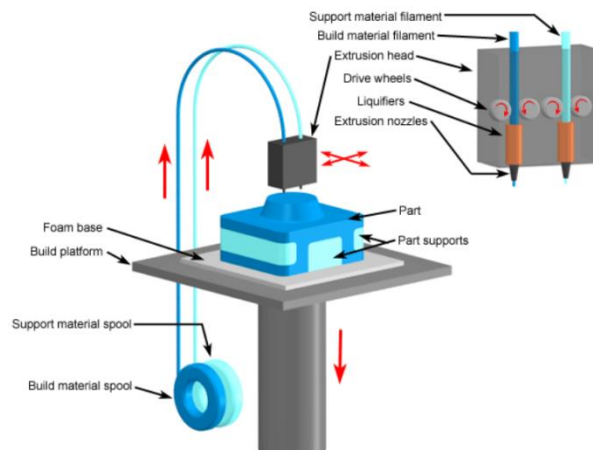


Figure 1.6: Material Extrusion process [26]

During the material extrusion process, the thermoplastic material, the filament, is pushed out of the heated nozzle as in Figure 1.6. The 3D printer prints the material on the printing table in this sequence; firstly the filament cools and then solidifies where it is printed. The 3D printer repeats this process based on the data from the print file, performing the printing process layer by layer. [27]

### 1.2.2.5 Material Jetting

Material Jetting (MJ) or “PolyJet” is an additive manufacturing process in which droplets of material are selectively deposited and cured on a printing table as shown in Figure 1.7. Using photopolymers or wax droplets that harden on exposure to light, objects build up one layer at a time. The nature of the Material Jetting (PolyJet) process allows different materials to be printed on the same object. In this technique, the aim is to create support structures from a different material to the produced model.[28]

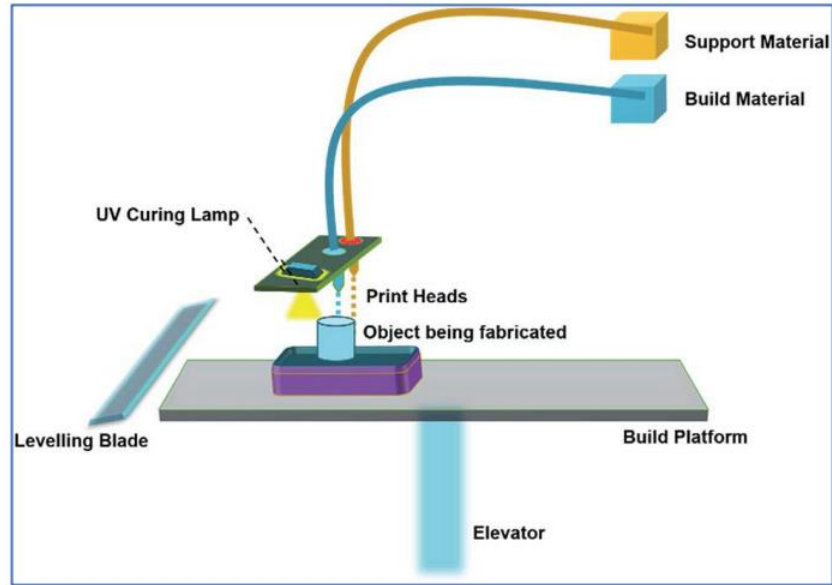


Figure 1.7: Material Jetting process [29]

### 1.2.2.6 Vat Photo Polymerization

Polymerization is an additive manufacturing process in which a light source selectively cures the photopolymer resin as shown in Figure 1.8. Also called Vat Polymerization, there are two most common forms of this method: SLA (Stereolithography) and DLP (Digital Light Processing).[30]

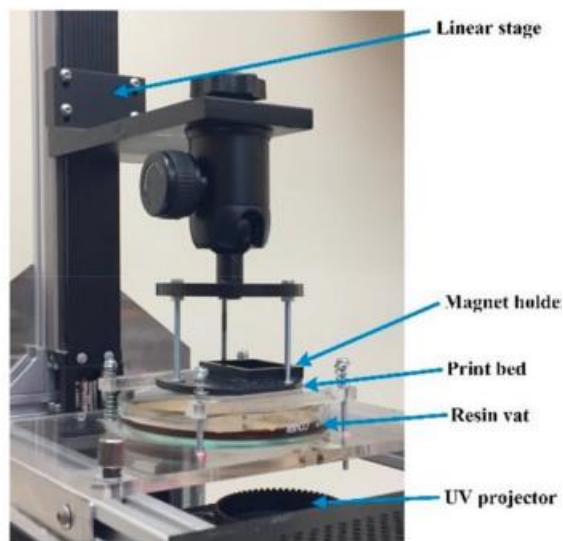


Figure 1.8: A sample SLA (Stereolithography) device [31]

The main difference between these two 3D printing technologies is the light source they use to cure the resin. SLA 3D printers use a dot laser as opposed to the voxel approach used in a DLP 3D printer.[31]

### 1.2.2.7 Binder Jetting

Binder Jetting technology was developed in 1993 at the Massachusetts Institute of Technology (MIT). Extrude Hone company licensed the patents from MIT in 1996 to manufacture metal parts using Binder jetting technology. In 2005, ExOne Company split from Extrude Hone, focusing on Binder Jetting of bronze-infiltrated stainless steel as well as pressed sands for metal casting molds. In 2021, Desktop metal acquired ExOne company. There are also other binder jetting companies such as Digital Metal, Voxeljet AG. [32]

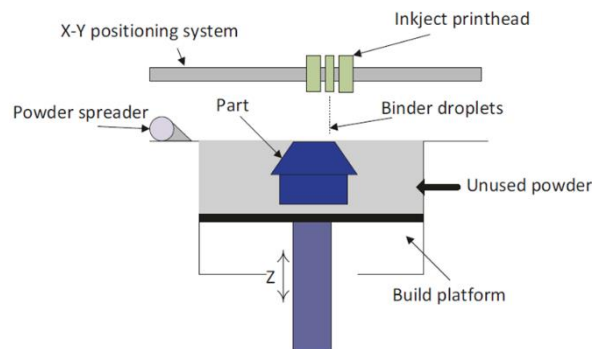


Figure 1.9: Schematic of the BJT process [32]

In binder jetting, there is a need for a 3D model of the part to be produced, designed with CAD programs. This CAD model is saved in STL format and sliced in layers with a slice program. As shown in Figure 1.9, a thin layer of powder is spread over the powder bed for printing and a new powder layer is compacted with the help of a counter-rotating roller. A liquid binder is sprayed onto the powder layer where the part will be formed, with the help of nozzles in the print head. After the penetration of the binder within the powder is complete, a heater passes over the powder bed to cure/dry. This process is repeated until the part is produced. [33]

The manufactured part is hardened in a furnace at low temperature around 200-220 °C and cleaned from dust. The hardened part is called “Green Part”. It is then sintered to improve mechanical properties in a high temperature sintering furnace as shown in Figure 1.10. at the appropriate temperature according to the manufacturing material.



Figure 1.10: A tube furnace for sintering

Sintering atmosphere, material composition, temperature and holding time are important parameters. Sintering methods are different for ceramics, metals and polymers. Ceramics have higher sintering temperatures and lower densification rates than metal powders.[34]

The surface roughness of the parts produced by the Binder Jetting method and subjected to secondary processes are not at the desired level. For this reason, various methods are used to increase the surface quality. The most commonly used techniques are sandblasting and polishing. It is also used in methods such as coating, machining, surface infiltration and hand polishing.[35]

The powder size and layer thickness used in all powder bed 3D printing methods directly affect the surface quality of the part. As the powder size and layer thickness increase, the surface quality decreases. However, as the powder size decreases, the fluidity ability of the powder decreases, making it difficult for the powder to spread to the build table at the time of printing. As the layer thickness increases, the processing time decreases and this reduces the costs. [36]

### 1.2.2.7.1 The Advantages of Binder Jetting

Table 1.1: The advantages and disadvantages of binder jetting

<b>Advantages</b>	<b>Disadvantages</b>
Cost effective	Secondary processes
Fast production time	Low relative density
Working environment	Surface roughness
No residual stresses	Shrinkage
No printing supports	
Homogeneity of microstructure	
Many eligible materials	

As it mentioned in Table 1.1, binder jetting is cost effective process because there is no necessity to use a heat source such as laser and coarse powders can be used in building of 3D parts, therefore; the production cost of fine powders reduces.[37] Moreover, it allows changing the properties of materials and the ratio of two types of materials to adjust the properties of the final parts, which means that there are unlimited possibilities for making components with binder jetting. It is a very suitable process for products with special requirements of the internal material structure.

Binder jetting allows fast production.[38] In fusion-based additive manufacturing technologies, the support material is produced together with the part. For this reason, it requires more time and material than in Binder Jetting technology.

Compared to other additive manufacturing methods, there is no need a controlled atmosphere for printing with binder jetting technology. It works at ambient temperature and in air.[39] Thus, problems related to oxidation, residual stress, separation and phase changes are not encountered. BJ technology is also suitable for production bigger part with more powder usage than other PBF technologies.

### 1.2.2.7.2 Disadvantages of Binder Jetting

Binder Jetting technology includes longer production processes due to the subsequent secondary processes (sintering, drying, etc.), It yields generally a lower relative density which is undesired. Density can be increased by a proper sintering, yet geometric distortions must be considered. [40]

When the BJ method and the PBF method are compared in terms of surface roughness, the parts produced with the Bj method appear to have lower resolution and higher surface roughness. [41]

There has not been enough work yet on secondary processes that the BJ method requires. Most of researches focused on sintering and infiltration. For this reason, post-production secondary processing strategies continue to be developed. [40]

### 1.2.3 Binder Jetting Parameters

There are many parameters that affect the properties of the parts to be produced with Binder Jetting technology. These parameters can be classified under 4 categories as it is shown in Table 1.2.

Table 1.2: Important parameters of binder jetting

Powder Parameters	Binder Parameters	Printing parameters	3D model design parameters
Chemical composition	Sprayability	Layer thickness	Design of overhang structure
Particle-size distribution	Wetting behavior	Powder-spreading and printing speed	
	Viscosity	Binder saturation	
Powder packaging	Binder volatility	Drying time	
Flowability		Heater power ratio	
Wettability		Print direction	

### 1.2.3.1. Powder Production Methods

The atomization method is a method used for powder production in all metals that have been melted. In this method; the molten metal flows through a hole in the bottom of the crucible, it is exposed to pressurized gas or liquid, and the liquid metal is solidified by breaking up into very fine particles. Atomization method can be classified in four main groups. [42]

- Water atomization
- Gas atomization
- Centrifugal atomization
- Plasma atomization

Metal powders for additive manufacturing are generally produced using the gas atomization process.[42]

Gas atomization is the process of separating the liquid metal into small droplets with the effect of gas flow with high velocities as illustrated in Figure 1.11. Liquid metal

droplets suddenly become spherical, cool and solidify. The diameters of these parts range from 1  $\mu\text{m}$  to 1 mm. Spherical metal alloy powders have superior properties due to the rapid solidification characteristic during processing. The microstructure of the powders formed is superior to the powders obtained by other methods. Gas atomization method is commonly preferred because of the controllable powder size and distribution. The purpose of the gas atomization method is to transfer the kinetic energy of the gas expanding at high speed to the liquid metal and to separate the metal into small droplets. The high-pressure gas atomization method is an effective method used in the production of fine metal and alloy powders.[43]

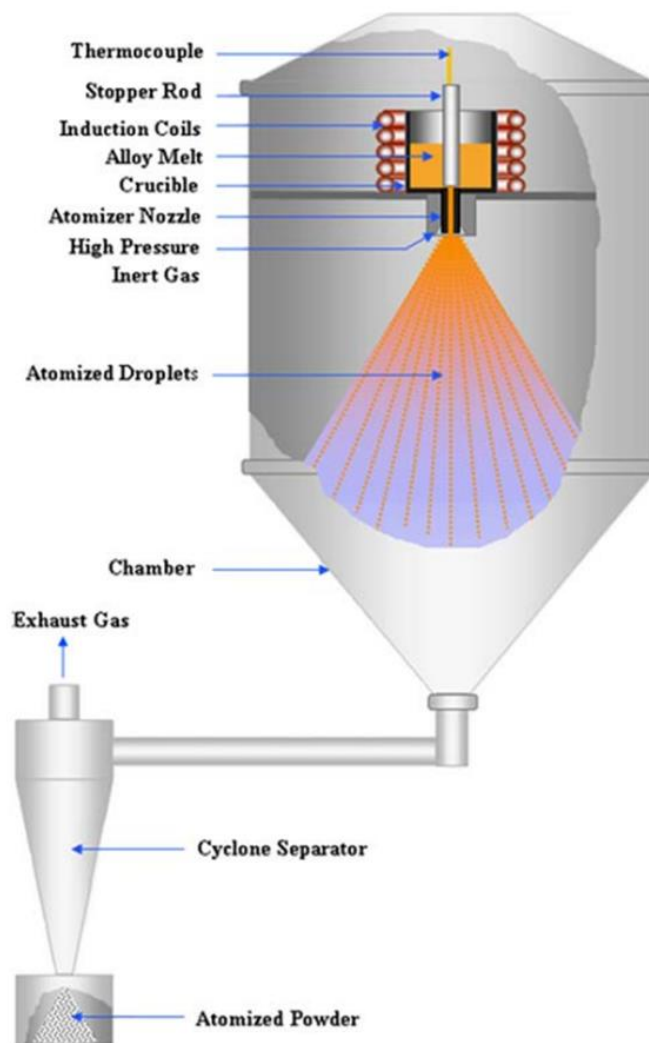


Figure 1.11: Schematic diagram of gas atomization processing [44]

Metal powders can also be produced with water atomization which is the other common atomization technique, however; water atomized powders have irregular shapes as shown in Figure 1.12. The sphericity of powders has a beneficial effect for powder spreadability, apparent and tap density, and therefore desired in metal AM processes. When gas atomization is compared with water atomization, spherical powders can be more easily produced.

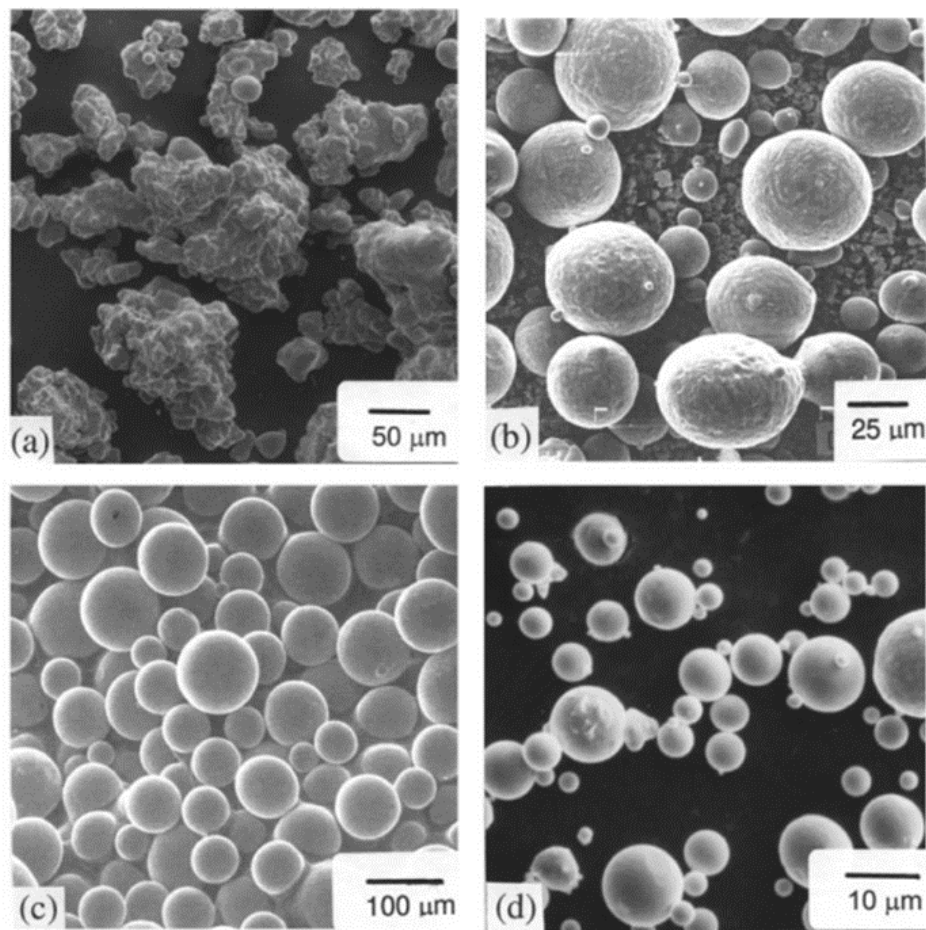


Figure 1.12: Scanning electron micrographs of atomized powders. (a) water atomized iron powder; (b) gas atomized high carbon steel; (c) centrifugally atomized nickel-base superalloy (plasma rotating electrode process); (d) vacuum atomized nickel-base superalloy [45]

Metal powders have a very important role in additive manufacturing processes. The geometry (spherical, prismatic, etc.), particle size distribution and morphology of the metal powder used will have a significant impact on the mechanical properties,

consistency observed from build to build, reproducibility, production of error-free components, manufacturing defects on surfaces.

The powder shape affects the parameters that directly affect the final part such as the powder's spreadability, powder packaging density, binder penetration time and density as indicated in Figure 1.13. Since the powders will be spread as a homogeneous, the spaces between the powder particles will be close to each other. The spherical powder shape also facilitates sintering as it increases powder-powder contact.[46]

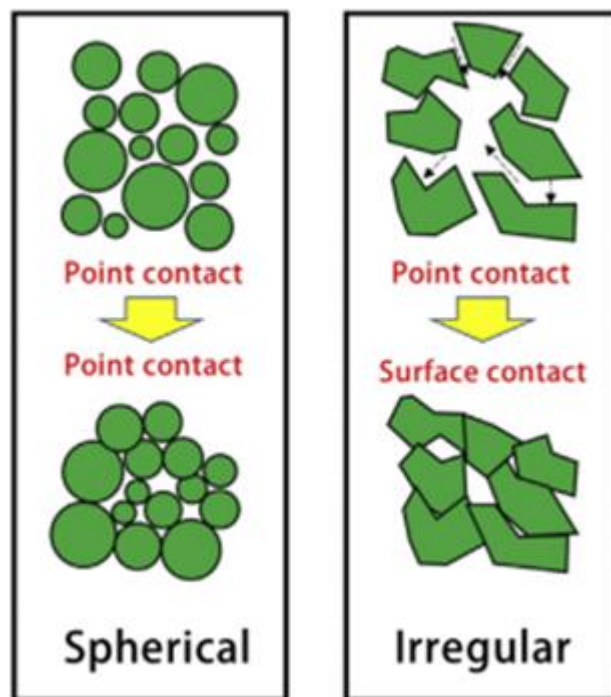


Figure 1.13: Changing mechanism of packing density of spherical and irregular ceramic powders after powder spreading [47]

Particle size distribution is an important point in additive manufacturing as it can affect many properties such as flowability of powder and ability to spread, powder bed density, energy input required to melt powders, and surface roughness [48]

As the powder particles get smaller, the fluidity of the powder decreases. However, powder binder interaction increases. The other effects of particle size distribution is layer thickness. The layer thickness must be greater than the largest particle size in the powder bed. For this reason, the smaller the powder size, the lower layer thickness and

the finer part enables production. The powder packaging also improves as the powder size increases.[47]

In the gas atomization process, all powder particles have the same chemical composition, but smaller particles tend to have a higher oxygen content due to their higher specific surface. In particular, the chemical composition will affect melting temperature, mechanical properties, weldability, thermal properties. Also, the chemical composition may change slightly after multiple uses in additive manufacturing machines. [49]

Powder packing density is an important parameter used to measure powder particle placement and maximum contact points. It is the density of each layer of powder spread through the roller. Powder morphology, powder size, interparticle strength, powder fluidity and powder surface chemistry are parameters that affect packaging density. Powder packing density then determines the final properties and geometric accuracy of the final part. [49]

#### 1.2.4 Binder Jetting Materials

Metallic materials are mostly used with Binder Jetting method in industrial applications. The metal materials used are conventional powder metallurgy alloys such as stainless steels.[50] As shown in Figure 1.14, copper and copper alloys, nickel and cobalt-based alloys, titanium alloys and stainless steels are studied as metallic materials, but high-density standard alloys are required in most industrial applications. This requirement has been met with various materials, but geometric accuracy after sintering is still one of the problems.[33] Inconel and cobalt-chromium alloys are very difficult to process with conventional methods, but these materials are much easier to process with the BJ method.

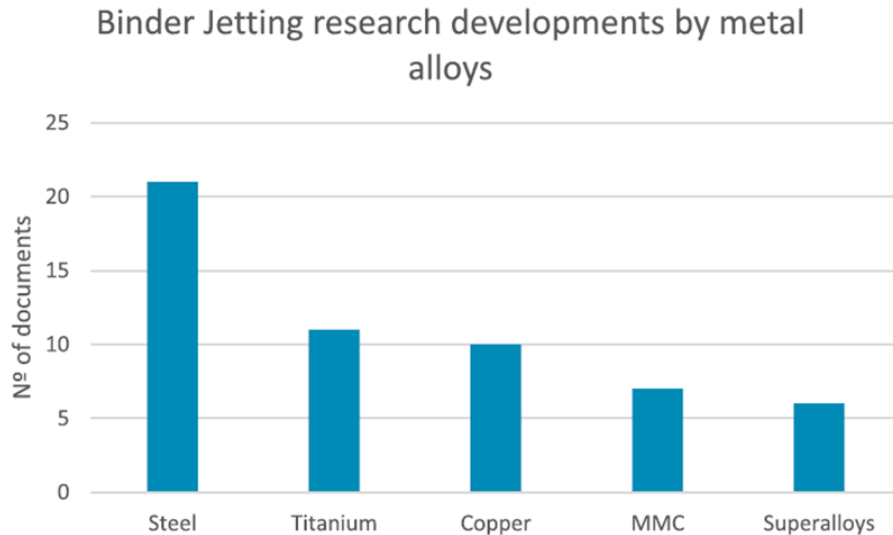


Figure 1.14: Scientific document amount related to binder jetting metal additive manufacturing reported in the literature [51]

The development of new powder binder systems is needed for the development of the Binder Jetting method in medical applications. Since biocompatibility is essential, the binders used during production must be biocompatible.[47]

Additive manufacturing of ceramic materials is more difficult than metals and polymers due to their high melting temperatures, high hardness and brittleness. Binder jetting is a more suitable additive manufacturing method for ceramic parts since melting is not performed compared to other powder bed additive manufacturing methods. Most of studies are focused on bio ceramics, structural ceramics and electric functional ceramics. [52]

### 1.2.5 Copper in Binder Jetting Technology

The physical and chemical properties of the materials used in the aviation, automotive and electrical industries are of great importance, therefore copper and copper alloys are widely used in these industries. [53] The thermal, electrical and corrosion resistance properties of copper and copper alloys are severely affected by impurities in them. Impurity can be prevented by special production methods, thus providing more stable physical and chemical properties. [54] Pure copper is widely used in aerospace, automotive and electrical fields due to its high thermal conductivity,

electrical conductivity and machinability. Especially pure copper is one of the main raw materials for heat exchangers and radiators, as shown in Figure 1.15, due to its high thermal conductivity.[55]

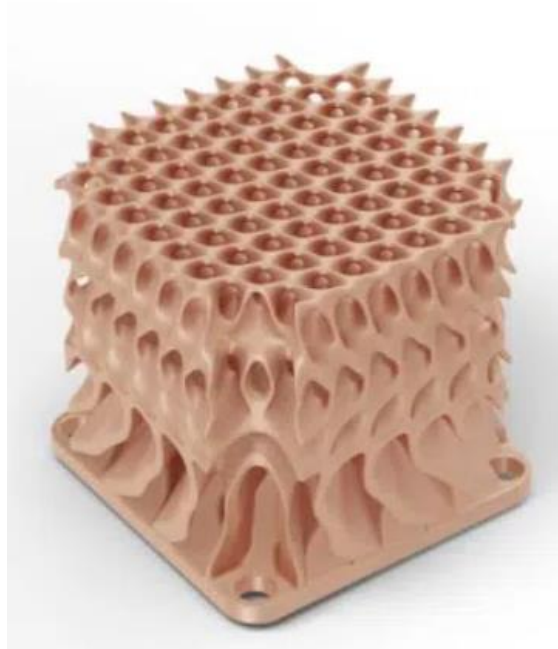


Figure 1.15: A DM Cu 3D printed a heat sink gyroid [69]

The demand for copper powder shows an increasing trend in the electrical and electronics industries. In addition, copper powder is a preferred metal powder for rapid prototyping and powder metallurgy applications. <100 Mesh copper powders have a market share of approximately 30% due to its low cost and wide availability, and an increase is expected with a growth of approximately 3.5% between 2019 and 2030. Accordingly, it is seen that the powders with 15-45 and 10-63 micron particle distribution used in this study are economically advantageous because binder jetting has advantageous such as fast processing then other additive manufacturing production techniques, and printing in complex shapes.

Recently, many researchers have been working with various additive manufacturing methods using pure copper to study the microstructure and properties. 3D printing setups for most metals use laser or electron beam and powder bed fusion processes. In this process, a flat bed of fine metal powder is selectively fused with an energy source, typically a very powerful laser. Subsequent layers of powder are similarly fused,

gradually creating a fully 3D object. While this process works quite well for many popular 3D printable metals such as aluminum, steel, nickel or titanium, the use of copper is very minimal.[56]

This problem is caused by the fact that 3D printing using the copper powder bed fusion process becomes quite difficult. Copper is highly reflective which defects optical mirror as shown in Figure 1.16, and conducts heat and electricity very well. Due to the insufficient power of the laser in fusion based additive manufacturing, copper parts can be produced with special laser (wave size suitable for copper reflection) or EBM (electron beam melting) benches, but due to the EBM vacuum environment, copper powder containing very low oxygen and hydrogen needs to be used as raw material. It is not a preferred method because it increases the cost of copper production. These two methods are considerably expensive for producing copper parts. [57]

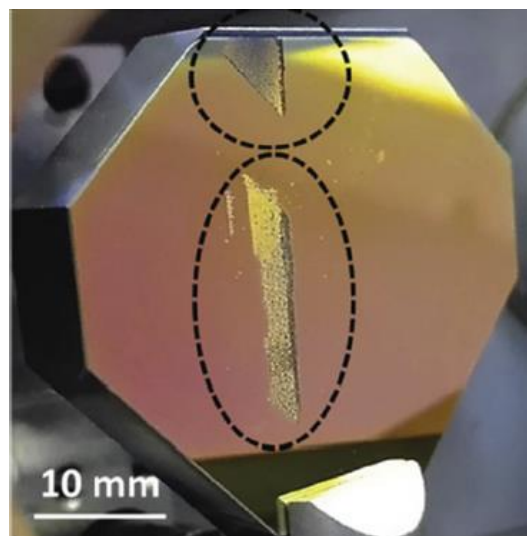


Figure 1.16: The damage to the optical mirror [56]

In order to eliminate these problems of copper, it is seen as a very suitable method for the production of pure copper parts as shown in Figure 1.17 with the binder jetting additive manufacturing method, which is a 3D printing technology with a high potential for use and has advantages such as serial, low operating cost and multiple productions. In addition, this additive manufacturing method does not need support structures compared to other additive manufacturing methods. [57]

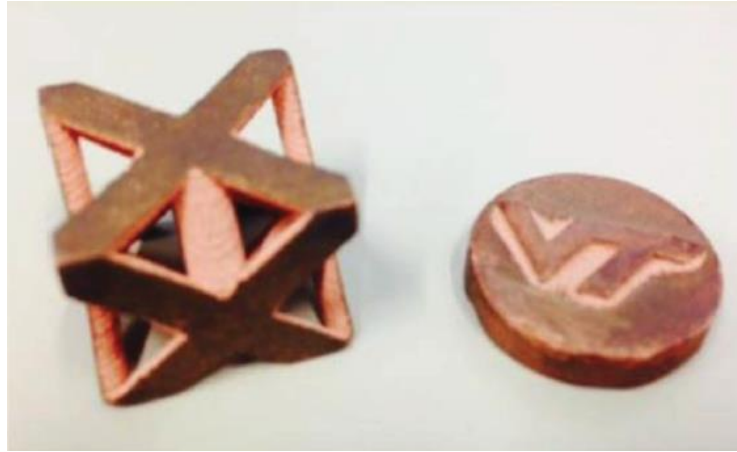


Figure 1.17: Complex-shaped copper made via binder jetting [56]

### 1.3 Literature Review

Bai et al. (2015) aimed to reveal the effect of bimodal copper powder mixtures on the properties of powder and sintered density of copper parts. As conclusion, decreasing of median size of powders has a benefit on apparent/tap density improvement in bimodal mixtures. Also, they found that apparent density yield result higher increase than tap density, and it is particularly useful for powder compaction on Binder Jetting. Another benefit of bimodal powders is green density of copper parts increased. [58]

Kumara et al. (2017) used gas atomized spherical shape copper powders due to its advantages, such as ease of powder recoating, better sintering, easier necking. They used two different copper powders which have median particle size of  $30\mu\text{m}$  and  $5\mu\text{m}$ , and mixed them to investigate the effects of hot isostatic pressing (HIP) on sintered bimodal powders parts. As a result of study, HIP process reduced the porosity and density of sintered bimodal parts increase 92% to 99.7%. [59]

Kumar and coworkers (2019) produced pure copper characterization samples with different particle size of powders to show the effects of porosity on the material properties with Binder Jetting. As a result, they found bimodal powders demonstrate highest density and material properties. The highest density of hipped bimodal part is 97.3%, tensile strength of 176MPa, thermal conductivity of  $327.9 \text{ W/m}\cdot\text{K}$  and an electrical conductivity of  $5.2 \times 10^7 \text{ S/m}$ . [60]

Miyanaji et al. (2020) studied about effect the fine copper powder on flowability and layer recoating for binder jetting additive manufacturing. In the study, they used copper powder that average particle size of around 5  $\mu\text{m}$  and compare the results with their previous study which average particle size of copper is around 20  $\mu\text{m}$ . As a result, they found an increase in density at least 9% when it is compared to the coarse copper powders. They, also found properties of parts with building with fine powders are greater than bimodal powder parts.[61]

Barthel and coworkers (2021) . investigate the effect of powder condition to understand the spreading parameters on green and sintered density. They used gas atomized stainless steel 316L with a particle size under 22  $\mu\text{m}$  (90%). In conclusion, powder drying has a benefit on the spreading parameters due to reduced powder cohesion and improved powder flowability. They also found, lower layer thickness and larger roller diameter increase packing stress per particle Thus, properties of green and sintered density both increases.[62]

Kwon et al. (2017) used two different stainless-steel powders and boron as a sintering agent in order to have fully dense final part. They compared the argon atmosphere sintering and vacuum sintering to see the effect sintering environment. Also, the hardness is compared with the cast stainless steel. As a result, the mixed powders had a better packing density because of better packing density distortion and shrinkage decreased and also surface finish improved. The vacuum sintering showed better density but surface oxidation occurred with sintering agent. The hardness values of the printed part by binder jetting reached the result of cast stainless steel. [63]

Otta et al. (2021) studied the effect of porosity and impurity of sintered copper on thermal properties. They used spherical and oxygen-free high conducting copper, then prepared a suspension which consist 56% copper. This suspension filled into silicon moulds and dried to have a green body. After that, the samples are sintered. As a conclusion, the porosity around 2-5% decrease the heat conductivity. On the other hand, the copper powder which include no impurity of iron has better heat conductivity. Thus, the main reason is the impurity in copper powder for low heat conductivity and prevention of impurities could give better heat conductivity even for low percentage of porosity. [64]

Enrique and coworkers (2018) aimed to produce metal matrix composite with in situ formation. They used Inconel 625 as matrix material and carbon from the binder as reinforced material. They also investigated the different sintering temperature routes. As a result, the formation of a core-shell structure occurred by using an inert atmosphere throughout the sintering process and Cr<sub>3</sub>C<sub>2</sub> phase composed the shell and the core was composed of a nickel matrix with NbC, Mo<sub>2</sub>C and Cr<sub>3</sub>C<sub>2</sub> phases. Argon atmosphere with 5% H<sub>2</sub> resulted in a core structure without the presence of the Cr<sub>3</sub>C<sub>2</sub> shell. [65]

Ming et al. (2021) aimed to study and demonstrate the feasibility of fabricating copper/diamond composite by binder jetting. Their main aim is to produce the part without any diamond graphitization. In order to understand the effect of the diamond volume, sintering temperature on density, porosity, they used copper-coated diamond powder and pure copper powder. The sintering is done at 800°C and 900°C. The results show that the diamond volume fraction has an important impact on sintering. When it increased from 10 vol% to 50 vol%, the sinterability decreased. Thus, the achieved highest sintered bulk density was 69.1% for 10 vol% Diamond and 65.6% for 50 vol% Diamond. [66]

Ming et al. (2021) investigated the effect of powder particle size on density properties. Seven different particle size alumina powders (from 0.05 µm to 70 µm) were used in this study. They found two conclusions, one of them is powder bed density and feed region density compatible under all conditions and apparent density has the strongest effect than tap density and Hausner ratio for powder bed density. [67]

# Chapter 2

## Materials and Methods

### 2.1 Experimental Studies

In order to understand the compatibility between copper powder and acrylic binder benchtop test were done. Benchtop test is manually mixing method of powder and binder. Different proportions of powder and binder were mixed and the most suitable mixture was casted into the bar to investigate the compatibility, curing and sintering behaviors. The results were compared with the samples produced by binder jetting.

### 2.2 Powder Preparation

In this study, gas atomized low oxygen and high oxygen content copper powders were used in order to see the effects of the oxygen content. Gas atomization produces spherical metal alloy powders and have superior properties due to the rapid solidification characteristic during processing, also lower oxygen content in the powder. However, the particle size distribution of these powders' ranges from 1  $\mu\text{m}$  to 1 mm. In addition, two different powder batches with different particle size distributions were used in order to observe the particle size effects. In order to have 15-45  $\mu\text{m}$  and 10-63  $\mu\text{m}$  particle size distribution, sieve and air classifier were used.

#### 2.2.1 Sieving

At first, both high oxygen and low oxygen containing copper powders were sieved from the 45 $\mu\text{m}$  sieve. After that, low oxygen containing copper powder is sieved from the 63 $\mu\text{m}$  sieve to see the particle size effects on the properties of final parts. In order to obtain <63 $\mu\text{m}$  and <45 $\mu\text{m}$  powders, an ultrasonic sieve is used at SentecBir

company. The sieving method is a technique used to produce the distribution of powders between 20 and 100 microns. The sieving generally made by ultrasonic sieving. During the sieving process, the particles accumulate between the stainless-steel sieve wires and close the pores. The cleaning problem is eliminated in the ultrasonic sieve system. Therefore, Ultrasonic Sieve as shown in Figure 2.1, is the most ideal solution.



Figure 2.1: An ultrasonic sieve

## 2.2.2 Air Classifier

In this study, air classifier is used to obtain 15-45  $\mu\text{m}$  and 10-63  $\mu\text{m}$  particle size distribution from the  $<63\mu\text{m}$  and  $<45\mu\text{m}$  low oxygen and high oxygen containing copper powders. Air classification (separation) is the process of separating the powders according to their size, shape and specific gravity by air flow and is carried out dry as shown in Figure 2.2. The separation process is characterized by average particle size of powders. Particles above average particle size of powders represent the "coarse" fraction, and those below the "fine" fraction. The performance of the separation is determined by the mass contents of each fraction in the resulting product.

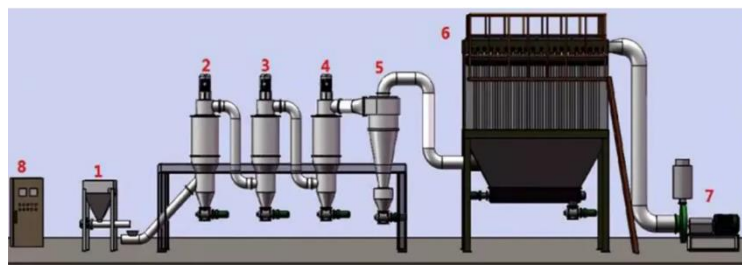


Figure 2.2: An illustration of air classifier 1. Feeding system, 2. Air Classifier-1, 3. Air Classifier-2, 4. Air Classifier-3, 5. Cyclone collector, 6. Dust collector, 7. Draught fan, 8. Electrical control system

Powders smaller than 5 microns may clog the nozzle of the inkjet print head during building in the binder-jetting device and cause insufficient binder deposition in production. For these reasons, particles below 10 microns have been eliminated in the classification of 15-45  $\mu\text{m}$  and 10-63  $\mu\text{m}$  powders. For better understanding, sample codes depending on powder properties are given in the Table 2.1.

Table 2.1: Representative sample coding

Sample code	Oxygen level	Particle size
LO-15-45	220 ppm	15-45
HO-15-45	1500 ppm	15-45
LO-10-63	230 ppm	10-63

## 2.3 Powder Characterization

Properties of a powder is great importance for the processing, transportation and storage of powder. While the shape and size properties of the powder play an important role in terms of good spreading to the powder bed, powder should be controlled in terms of its homogeneity, good flow and density properties.

### 2.3.1 Helium pycnometry

In this study, Micromeritics AccuPyc II 1340 helium pycnometer at İzmir Katip Celebi University, was used in order to find the true density values of the powders (in Figure 2.3). Helium pycnometer aims to find volume and true density using Archimedes' fluid overflow principle and Boyle's Law. For maximum accuracy of measurements, the overflowing fluid must be an inert gas that can enter all but the smallest pores. Therefore, Helium gas with small atomic dimensions approaching pores with a diameter of 0.25 nm is considered suitable for measurements. Helium's behavior as an ideal gas is also a reason for preference.



Figure 2.3: Micromeritics AccuPyc II 1340 helium pycnometer

### 2.3.2 Particle size analyzer

The sieved and classified powders' particle size distributions were analyzed with Malvern mastersizer 2000 as shown in Figure 2.4, at SentesBir R&D laboratory. Both Sieved copper powders ( $<63\mu\text{m}$  and  $<45\mu\text{m}$ ) and air classified copper powders ( $15\text{-}45\mu\text{m}$  and  $10\text{-}63\mu\text{m}$ ) were analyzed. It has been seen that the copper powders of which particle sizes are  $15\text{-}45\mu\text{m}$  and  $10\text{-}63\mu\text{m}$  do not contain powder with less than 7 micron sizes.



Figure 2.4: Malvern Hydro 2000

### 2.3.3 Apparent Density and Flow Measurement

Apparent densities and flow properties of both high and low oxygen containing copper powders were measured in order to understand the effect of apparent density on final density of the sintered part. All tests are done by hall flowmeter as illustrated in Figure 2.5, at SentesBir R&D center according to the ASTM B212 – 13 standard. The flow properties of the powders were measured with ASTM B213-20 standard using the Hall-flowmeter.

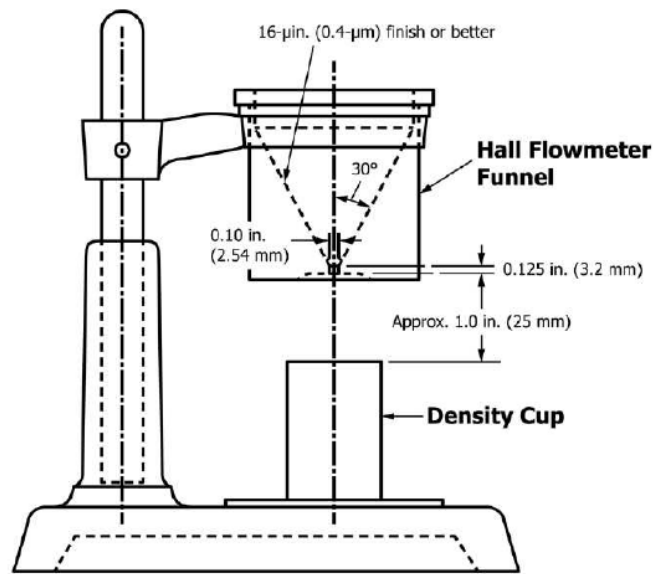


FIG. 1 Flowmeter Apparatus — Hall Funnel

Figure 2.5: The standard schematic of flowmeter apparatus — Hall Funnel

### 2.3.4 Tap Density Measurement

Tap density of the powders were measured in accordance with ASTM B 527 – 93 standard (Determination of Tap Density of Metallic Powders and Compounds) using the apparatus as shown in Figure 2.6.

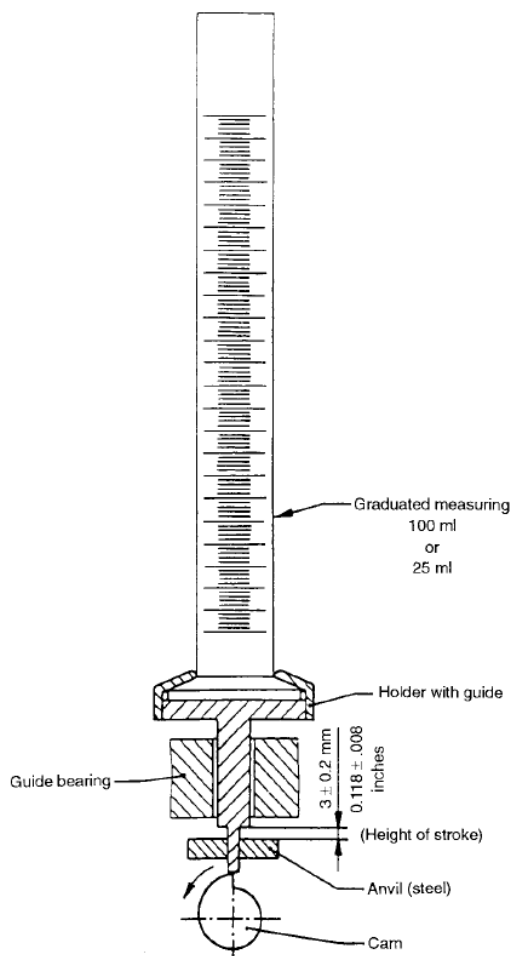


Figure 2.6: Example of Tapping Apparatus

### 2.3.5 Elemental analyzer

Elemental analysis was carried out in order to examine the effects of the oxygen and carbon ratio of the copper powders on the sintered final part. In Figure 2.7, Leco TC 400 and Eltra Elemental C/S instruments of Sentebir AS were used for oxygen and carbon analysis.



(a)



(b)

Figure 2.7: (a) Eltra Carbon/Sulphur analyzer, (b) Leco oxygen/nitrogen analyzer

### 2.3.6 SEM analyses

SEM pictures of three different powders were taken at the Thermo Scientific Apreo S from Ege University Central Research Test and Analysis Laboratory Application and Research Center



Figure 2.8: Scanning electron microscope (SEM)

## 2.4 Binder Jetting Production Procedure

In order to understand the shrinkage behavior, firstly, cube samples with a volume of 8 m<sup>3</sup> were printed with a low oxygen content of 15-45 μm. The dimensions of all characterization samples were printed with considering shrinkage.

### 2.4.1 3D Cad Model

In this step, the geometry of the all-characterization samples, as shown in Table 2.2, are designed in CAD program. Then the dimensions of the samples were determined. Dimension of the samples are shown in table 3 and table 4 and the tensile test samples are designed according ASTM E8/E8M-16a as shown in Figure 2.9 and in Table 2.3. Since the part must be designed with computer aided design programs and this design must be ready for 3D printing, the modeling step, which is the first step, has been examined under two headings, the creation of the CAD model and the STL file.

Table 2.2: Diameter of characterization samples

Samples	Cu Powder	Number of samples
Tensile Test Samples (below)	Low Oxygen (15-45 $\mu$ m)	6
Electrical Conductivity Test Samples (r:6,6 mm, length:77 mm), cylinder	High Oxygen (15-45 $\mu$ m)	5
Cube-shaped Samples (8,8 mm <sup>3</sup> )	Low Oxygen (10-63 $\mu$ m)	8
Surface Roughness Test Samples (r:11mm, length: 2,2 mm) Circle		4

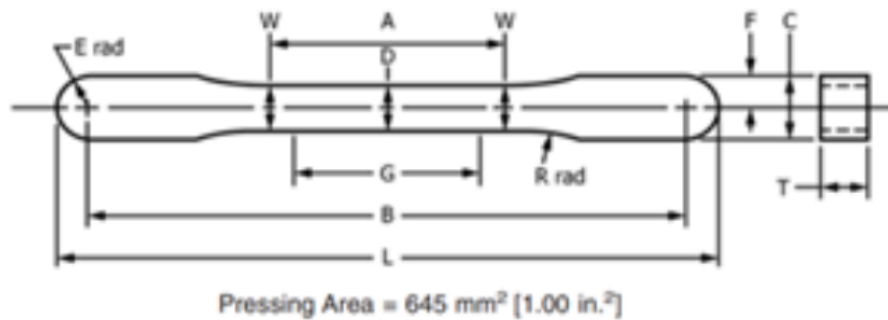


Figure 2.9: Design of tensile stress sample (ASTM E8/E8M-16a)

Table 2.3: Diameter of tensile test samples

<b>Dimensions (mm)</b>	
G	28
D	6,3
W	6,6
T	6,6
R	28
A	35
B	89,1
L	98,6
C	9,6
F	4,8
E	4,8

### 2.4.2 Layer Thickness and Binder Saturation

As the layer thickness increases, the surface quality decreases. On the other hand, as the layer thickness decreases, the printing time increases, but when the part prints thinner layers, the surface quality increases. Excessive amount of binder may affect previous powder layers due to the penetrating properties of binders. During printing, the capillary effect may cause the binders to leak into neighboring powders, so it is very important to apply an optimum level of binder during printing. If the amount of binder is more than the optimum level, it causes excessive spread in the powder bed. This causes poor surface quality and poor geometric accuracy.

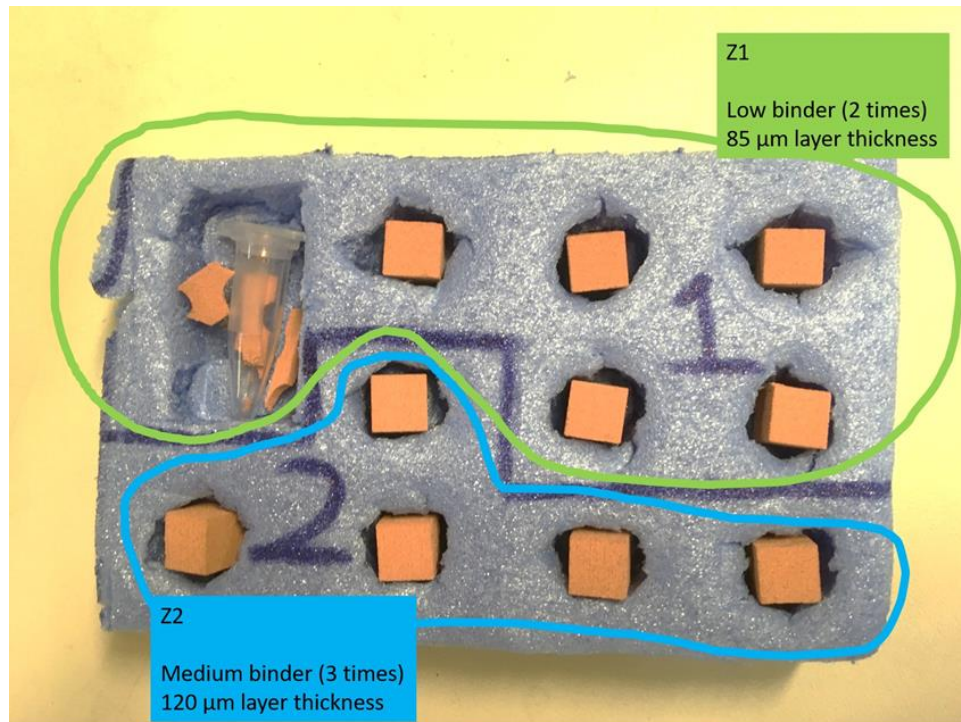


Figure 2.10: Cube samples produced with binder jetting

For the reasons mentioned above, the effect of layer thickness and binder saturation was investigated by printing 8m3 cube samples which 10-63  $\mu\text{m}$  powder used for both the low binder and 85  $\mu\text{m}$  layer thickness, and the medium binder and 120  $\mu\text{m}$  layer thickness parameters, as shown in Figure 2.10.

## 2.5 Effect of Sintering Atmosphere and Temperature

After the printing process, the sintering process is carried out to remove the binder from the printed parts and to ensure that the voids disappear and become solid. There are factors to be considered in determining the desired properties of the parts produced by binder jetting. These are sintering atmosphere, temperature and sintering time. It is very important to control the sintering process as each material has its own sintering properties.

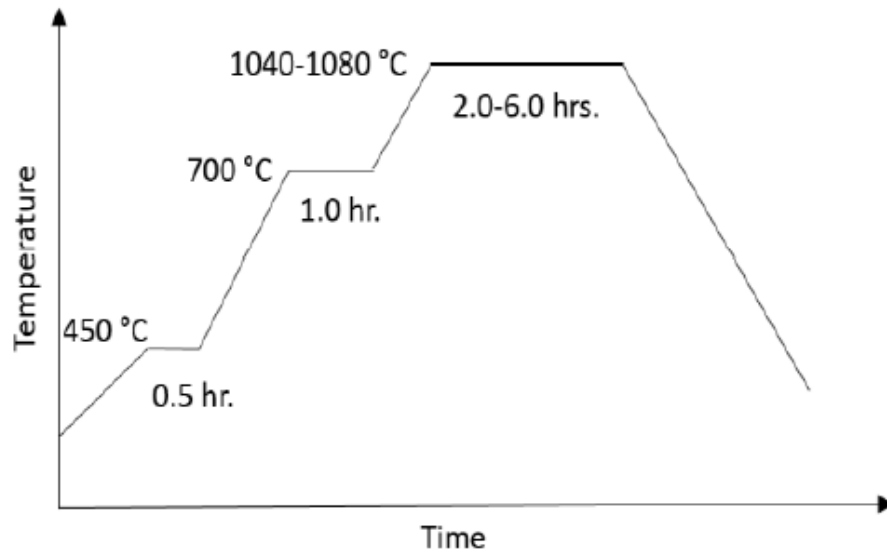


Figure 2.11: Sintering Regime [68]

In this study, the effect of sintering atmosphere was investigated by using different gases such as 100% nitrogen, 95/5% nitrogen/hydrogen and 100% hydrogen. In addition, the effect of sintering temperature was investigated by sintering at different sintering temperatures of 1040C, 1050 and 1070C as shown in Figure 2.11 which is similar the heating schedules that Bai et al used. In addition to these, the effects of deoxidation step and debinding temperature were investigated. Finally, the effects of sintering speed and time were examined. All these tests were carried out in a tube furnace located in SentesBir R&D center as shown in Figure 2.12.



Figure 2.12: Protherm tubular furnace

## 2.6 Characterization Techniques

### 2.6.1 Density, Porosity and Shrinkage of Samples

Densities of sintered cube samples were measured with mass/volume formula by using a caliper and the ASTM B 962 – 08 standard (Density of Compacted or Sintered Powder Metallurgy (PM) Products Using Archimedes' Principle), but the density after curing was measured with the standard mass/volume formula. This is because cured samples still contain binder and can be easily oxidized in water.

In Archimedes principle, sintered cube samples were first impregnated in silicone oil. Afterwards, the excess silicone oil on the surfaces was cleaned with a cloth impregnated with silicone oil, and density measurements were made on a calibrated precision balance with an Archimedean test apparatus in SentesBir R&D center.

Finally, the shrinkage of the samples whose densities were measured after sintering and after curing were calculated.

### 2.6.2 Microstructure characterization

As a result of the previous benchtop tests, it was observed that the samples prepared by hot molding were oxidized due to the temperature. For this reason, sintered samples for microstructural analysis were molded using the acrylic cold molding resin, hardener and cold molding apparatus shown in the Figure 2.13.

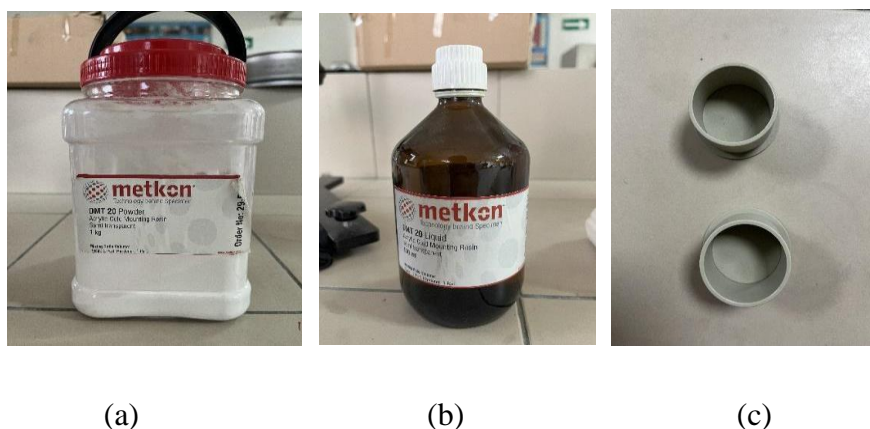


Figure 2.13: (a) acrylic cold mounting, (b) hardener, and (c) mould.

Afterwards, grinding was applied to the specimens removed from the cold mold. The grinding process was done with the automatic grinding machine in SentesBir R&D center as shown in the Figure 2.14. SiC papers with coarse grinding was used as the first step, and then grinding was continued with 600 grid and 1200 grid papers. After the samples had a flat surface, the polishing process was started. 3  $\mu\text{m}$  and 1  $\mu\text{m}$  diamond solution was used in the polishing process, then the process was completed by polishing with colloidal silica.



Figure 2.14: Automatic grinding & polishing machine

In order to analyze the porosity of the polished parts, NICON Eclipse Optical Microscope, located in SentesBir R&D center, was used with 2,5x, 5x and 10x magnification. The optical microscope used is shown in Figure 2.15.



Figure 2.15: Nikon Eclipse Optical Microscope

In the next step, the results of the porosity analysis with an optical microscope were analyzed using the ImageJ software, and the porosity densities were calculated. These results were then compared with the Archimedean densities.

In final next step, the polished samples, which were then analyzed for porosity, were etched for microstructural analysis. The etching solution was etched with the etching solution No. 27 in the ASTM-E407-07 Microetching Metals and Alloys standard, and microstructure analysis was performed.

### 2.6.3 Surface Roughness

Surface roughness of samples were measured with Profilometer in Dokuz Eylül University as seen in the Figure 2.16.



Figure 2.16: Linear Profilometer

### 2.6.4 Tensile Tests

Tensile tests of the samples produced with binder jetting were applied in accordance with ASTM -E8/E8M - 16a standards using Shimadzu machine at Dokuz Eylül University Mechanical Engineering Dept. Composites Laboratory as shown in Figure 2.17.



Figure 2.17: Shimadzu Tensile test machine

## 2.6.5 Electrical Conductivity Tests

The electrical conductivity test samples produced with binder jetting were tested with 4 point measurements at Izmir Katip Çelebi University as shown in Figure 2.18. The electrical conductivity of all samples were calculated by the Pouillet's Law with the results of electrical resistivity.

The electrical resistivity ( $\rho$ ) was calculated from the equation Pouillet's Law formula below:

$$\rho = R \frac{A}{\ell} \quad (2.1)$$

In equation, ( $\rho$ ): Resistivity, (A): Cross-section Area , (L): Length, (R) Resistance over Length.

$$\sigma = \frac{1}{\rho} \quad (2.2)$$

The electrical conductivity ( $\sigma$ ) was calculated from the equation above.



Figure 2.18: 4-point measurements apparatus

# Chapter 3

## Results and Discussion

### 3.1 Benchtop Test Results

Before starting the additive manufacturing step, benchtop tests were done in order to observe the compability of the binder-powder, and also curing and sintering behaviors.

#### 3.1.1 Importance of Binder Ratio

Table 3.1 represents the mixing ratio of binder and copper powder that has  $<63 \mu\text{m}$  particle size. Mixture1 which has 3% binder content showed easily crumbling structure and has low castability. On the other hand, mixture 4 and 5 (having binder ratios of 7-8%) showed very low viscosity, and was difficult to be casted.

The best results were obtained with mixture 2 and 3, which were contain of 5 and 6% binder ratio. The mixtures had appropriate viscosity to cast into bars. Therefore, all benchtop tests were done using mixture 2. Mixture 3 was elected because higher binder ratio could negatively effect the sintered density by leaving higher porosity in the structure.

Table 3.1: Powder and binder ratios for benchtop test mixtures

	<b>Mixture 1</b>	<b>Mixture 2</b>	<b>Mixture 3</b>	<b>Mixture 4</b>	<b>Mixture 5</b>
Low O2 Cu Powder (%)	97	95	94	93	92
Acrylic Binder (%)	3	5	6	7	8

### 3.1.2 Curing Behavior

In order to observe the curing behavior of the binder, the mixture 2 was casted into a rectangular bars made of steel, as shown in Figure 3.1 (a). Then, the bars have been put into the furnace for curing at 200 °C for 2 hours. After curing, it was seen that the cured mixture has been stuck on the bar and some cracks have been observed. The cured sample could be removed from the bar only by shredding, as shown in Figure 3.1 (b).



(a)



(b)

Figure 3.1: (a) Cured sample in the bar (200 °C for 2 hours), (b) Cured sample in pieces.

Another test was done to evaluate the effect of the bar material. Cylindrical bars that are made of steel, graphite and composite, as shown in Figure 3.2, were used. The results were similar with the rectangular bar, as the cured parts have been stuck, cracks occurred and the only way to took of parts was to shred.



(a)



(b)



(c)

Figure 3.2: (a) cured part in steel bar (b) cured bar in carbon bar (c) cured part in fiber bar.

Finally, the mixture 2 is cured in silicon bars at 200 °C for 2 hours as shown in Figure 3.3. It is seen that silicon bar is more appropriate as the molding material since the samples easily have been took off from the bars more easily. However, it should be noticed that the cubes were oxidized as the curing was conducted in open atmosphere.

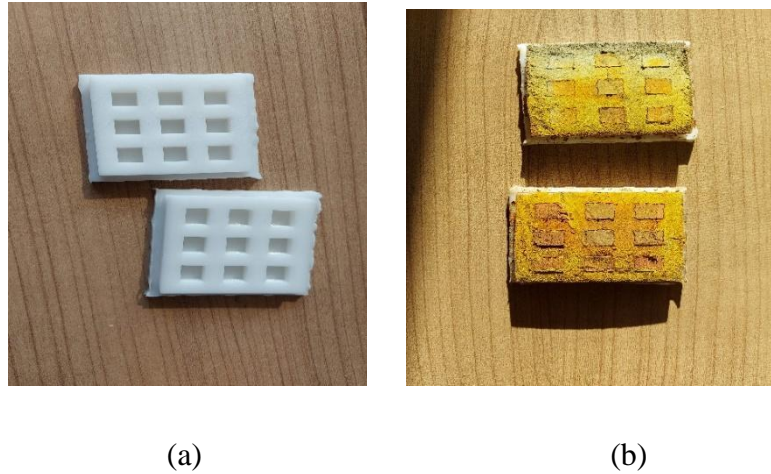


Figure 3.3: (a) Silicon bars, (b) Cured bars at 200 °C for 2 hours.

In order to overcome the oxidation, the mixture 2 has been casted into silicon bars and cured in the tube furnace under Argon atmosphere at 200 °C for 2 hours, as shown in Figure 3.4 (a). As shown 3.4 (b), curing was found to be successful because it is seen that oxidation is eliminated using argon atmosphere.

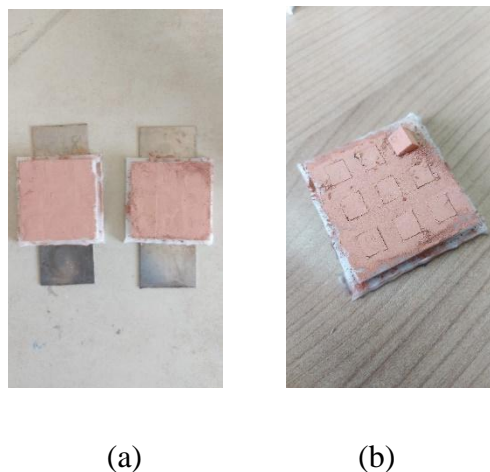


Figure 3.4: (a) Benchtop test samples before curing, (b) Benchtop test samples after curing in argon atmosphere.

All the cured benchtop test samples were sintered with binder jetting method, and the results are given in the sintering optimization section of the thesis.

## 3.2 Powder Characterization Results

In the comparing the benchtop test samples with binder jetting samples, the binder jetting samples were printed with  $<45\ \mu\text{m}$  low oxygen copper powders. It was observed that the fine powders blocked the binder-spraying nozzle during spreading and the production was prolonged. Therefore, the copper powders were prepared not to contain powders under  $7\ \mu\text{m}$ .

For the first set of powders ( $15\text{-}45\ \mu\text{m}$ ),  $106\ \mu\text{m}$  copper powders with low oxygen content were sieved from  $45\ \mu\text{m}$  sieve and then classified as  $15\text{-}45\ \mu\text{m}$  and the prepared copper powders did not contain any powders under  $7\ \mu\text{m}$  as shown in Figure 3.5 (a).

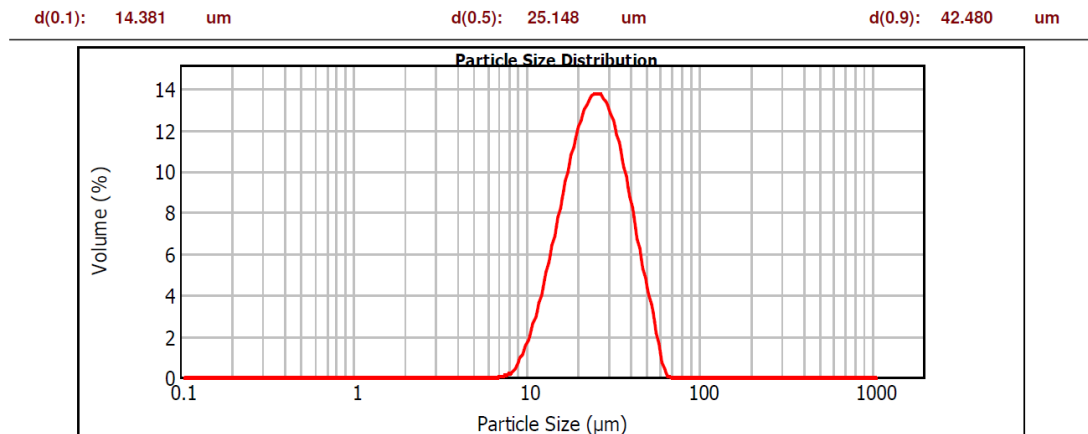
In order to find the effect of powder oxygen content,  $<106\ \mu\text{m}$  coppers powders with high oxygen content were sieved from  $45\ \mu\text{m}$  sieve and then classified as  $15\text{-}45\ \mu\text{m}$  as shown in Figure 3.5 (b).

In order to find the effect of particle size distribution,  $<106\ \mu\text{m}$  coppers powders with low oxygen content were sieved from  $63\ \mu\text{m}$  sieve and then classified as  $10\text{-}63\ \mu\text{m}$  as shown in Figure 3.5 (c). The average particle size values of LO-15-45 and LO-10-63 powders are 25.1 and 33.9 microns, respectively.

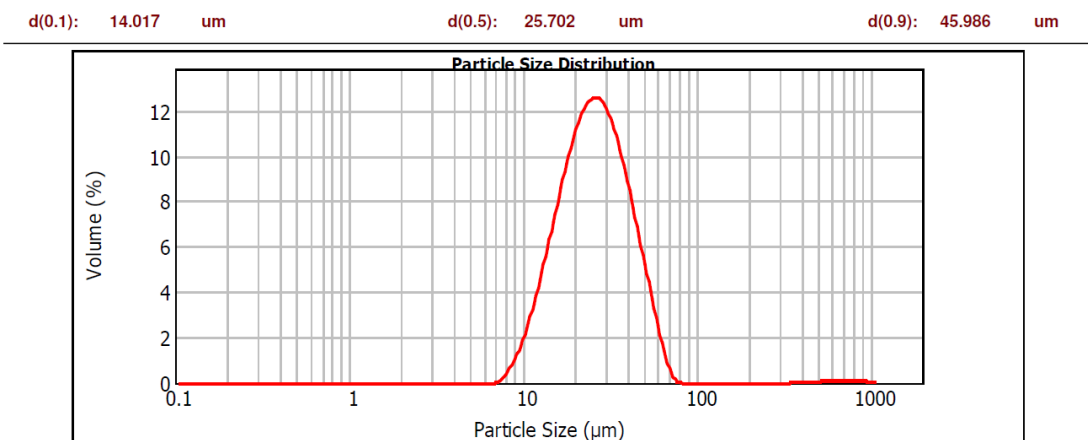
In Table 3.2, apparent density, tap density, true density, flow rate, oxygen and carbon content of all the powder batches were given. When LO-15-45 and HO-15-45 are compared, it is seen that true density and apparent density values of high-oxygen powders are lower than low-oxygen powders. The true density and the apparent density of low-oxygen powder is lower because of its higher oxygen content (1500 ppm). This can be attributed to the presence of copper-oxide since oxide has lower density than Cu.

When LO-15-45 and LO-10-63 are compared, apparent density of LO-15-45 is higher because the sphericity and the flow rate of LO-15-45 is lower than HO-15-45 and LO-10-63, which could be because of the difference in the sphericity of the powder batches.

SEM images of the three different powder batches are shown in Figure 3.6. It is seen that LO-15-45 and HO-15-45 powder batches contain higher amount of smaller particles and powder distributions are relatively smaller compared to LO-10-63 powder.

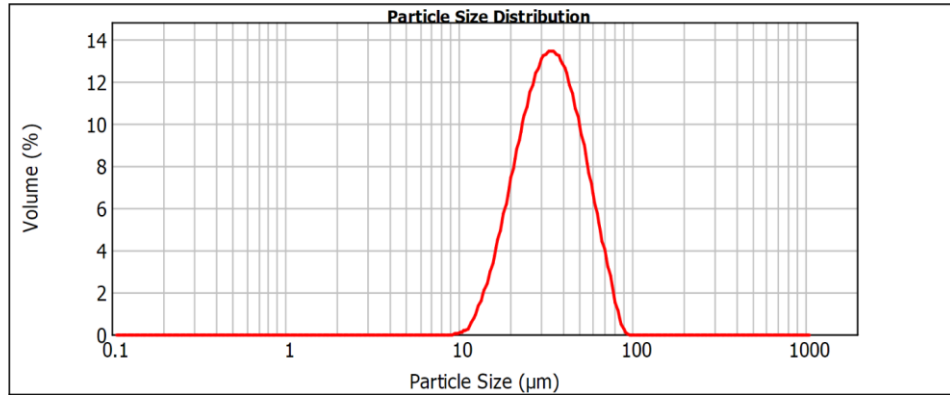


(a)



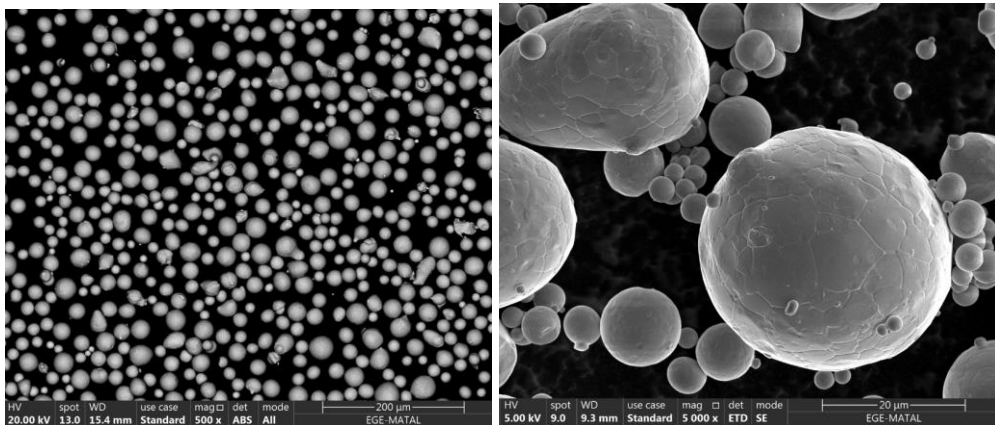
(b)

d(0.1): 10.289 um                      d(0.5): 33.866 um                      d(0.9): 62.065 um



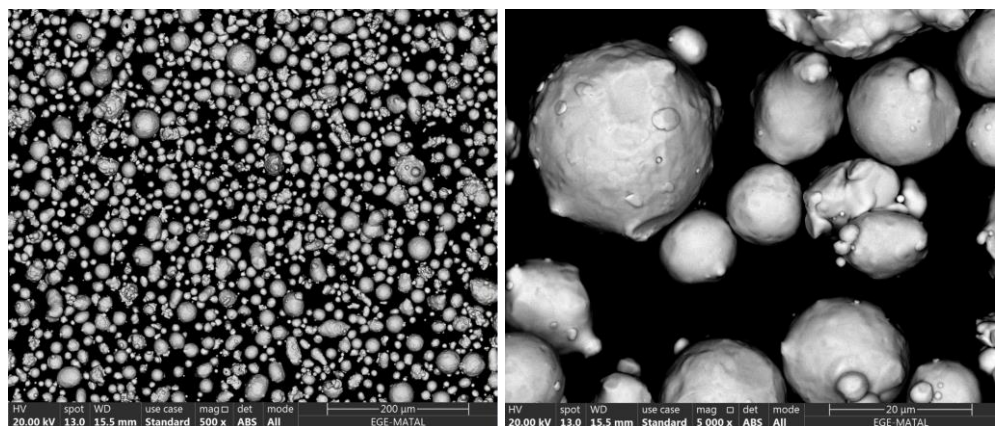
(c)

Figure 3.5: (a) Particle size distributions of 15-45  $\mu\text{m}$  low oxygen, (b) 15-45  $\mu\text{m}$  high oxygen, c) 10-63  $\mu\text{m}$  low oxygen copper powders



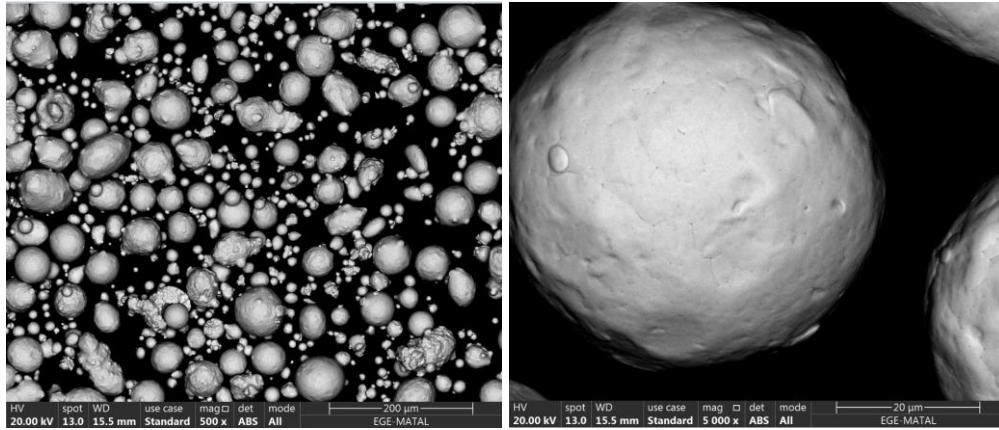
(a)

(b)



(c)

(d)



(e)

(f)

Figure 3.6: SEM images of lower and higher magnifications of (a,b) 15-45  $\mu\text{m}$  low oxygen powders, (c,d) 15-45  $\mu\text{m}$  high oxygen powders, and (e,f) 10-63  $\mu\text{m}$  low oxygen powders

Table 3.2: Powder characterization results of the all copper powders. The results were added by averaging as a result of five consistent measurements

Characterization of Copper Powders	LO-15-45	HO-15-45	LO-10-63
Apparent Density ( $\text{g}/\text{cm}^3$ )	5,04	4,54	4,72
Tap density ( $\text{g}/\text{cm}^3$ )	5,15	5,2	5,49
True density ( $\text{g}/\text{cm}^3$ )	8.8965	8.7934	8.8972
Flow rate (s/50 g)	11,28	15,23	15,44
O <sub>2</sub> content (ppm)	220	1500	230
Carbon content (ppm)	300	42	320

### 3.3 Sintering Parameter Optimization Results

#### 3.3.1 Effects of Sintering Temperature on Density

In Table 3.3, the cube samples produced with benchtop test and binder jetting sintered under 95/5% nitrogen/hydrogen atmosphere with a sintering regime, which contains debinding at 450 °C for 30 minutes, oxidation-reduction at 700 °C for 1 hour and sintering at 1040 °C for 130 minutes with 5°C/min as shown in Figure 25. It is seen that binder-jetting samples showed higher relative density. One important point is that benchtop test gives close density values compared to commercial binder jetting process.

Table 3.3: Comparison of benchtop test and binder jetting samples at 1040 °C for 130 min. under 5% hydrogen and 95% nitrogen atmosphere

<b>Particle Size/Production Method</b>	<b>Sintered temp./time</b>	<b>Sintered Bulk Density (gr/cm<sup>3</sup>)</b>	<b>Relative Density-Archimedes (%)</b>
<45 µm/(Benchtop)	1040 °C /130 min.	4,82 ±0,7	53,74 ±2
<45 µm/(Binder Jetting)	1040 °C /130 min.	4,88 ±0,6	54,41 ±2

In Table 3.4, the cube samples produced with benchtop test and binder jetting sintered under 95/5% nitrogen/hydrogen atmosphere with a sintering regime, which contains debinding at 450 °C for 30 minutes, oxidation-reduction at 700 °C for 1 hour and sintering at 1050 °C for 130 minutes with 5°C/min as shown in figure 25. It is observed that the relative densities of samples increased with the increase in temperature samples.

Table 3.4: Comparison of benchtop test and binder jetting samples at 1050 °C for 130 min. in 95/5% nitrogen/hydrogen atmosphere

<b>Particle Size/Production Method</b>	<b>Sintered temp./time</b>	<b>Sintered Bulk Density (gr/cm<sup>3</sup>)</b>	<b>Relative Density (%)</b>
<45 μm/Sample 1 (Benchtop)	1050 °C /130 min.	4,77 ±0,9	52,79 ±1,9
<45 μm/Sample 2 (Binder Jetting)	1050 °C /130 min	5,01 ±0,8	55,74 ±1,8

In Table 3.5, the sintering regime used as similar in table 6 and 7. It is seen that increasing the temperature from 1050 °C to 1070 °C had a beneficial effect on density.

Table 3.5: Comparison of benchtop test and binder jetting samples at 1070 °C for 130 min. in 95/5% nitrogen/hydrogen atmosphere

<b>Particle Size/Production Method</b>	<b>Sintered temp./time</b>	<b>Sintered Bulk Density (gr/cm<sup>3</sup>)</b>	<b>Relative Density (%)</b>
<45 μm/Sample 1 (Benchtop)	1070 °C/130 min.	4,84 ±0,8	54,01 ±2,1
<45 μm/Sample 2 (Binder Jetting)	1070 °C/130 min.	5,28 ±0,6	58,97 ±1,6

As a result, sintered of benchtop test samples and binder jetting samples showed different relative densities but an increase in temperature resulted better relative densities for all samples.

### 3.3.2 Effects of Binder Ratio on Density

In order to understand the effects of binder ratio and layer thickness, the cube samples printed with 15-45  $\mu\text{m}$  low oxygen copper powders by binder jetting at Istanbul Technical University EKAM Research Center. The samples sintered with a sintering regime, which is debinding at 450 °C for 30 minutes, oxidation-reduction at 700 °C for 1 hour and sintering at 1070 °C for 130 minutes with 5°C/min in 95/5% nitrogen/hydrogen atmosphere.

Table 3.6: Sintering results of samples that printed with the parameter of low binder/85  $\mu\text{m}$  layer thickness and medium binder/120  $\mu\text{m}$  thickness

<b>Binder Ratio</b>	<b>Sintering temp./time</b>	<b>Sintered Bulk Density (gr/cm<sup>3</sup>)</b>	<b>Relative Density (%)</b>
Low binder	1070/130 min.	5,93 $\pm$ 0,5	66,2 $\pm$ 1,3
Medium binder	1070/130 min.	5,62 $\pm$ 0,6	62,7 $\pm$ 1,5

As it seen in Table 3.6, the low binder content results in better relative density. Therefore, low binder content with 85- $\mu\text{m}$  thickness parameter was chosen as the printing parameter, and all other samples were printed with this parameter.

### 3.3.3 Effects of Sintering Atmosphere on Density

The 15-45  $\mu\text{m}$  low oxygen copper cubes sintered with the similar sintering regime (debinding at 450 °C for 30 minutes, oxidation-reduction at 700 °C for 1 hour and sintering at 1070 °C for 130 minutes with 5°C/min.) but different atmosphere. As it can be seen in the Figure 3.7, 100% H<sub>2</sub> atmosphere have a positive effect on the density.

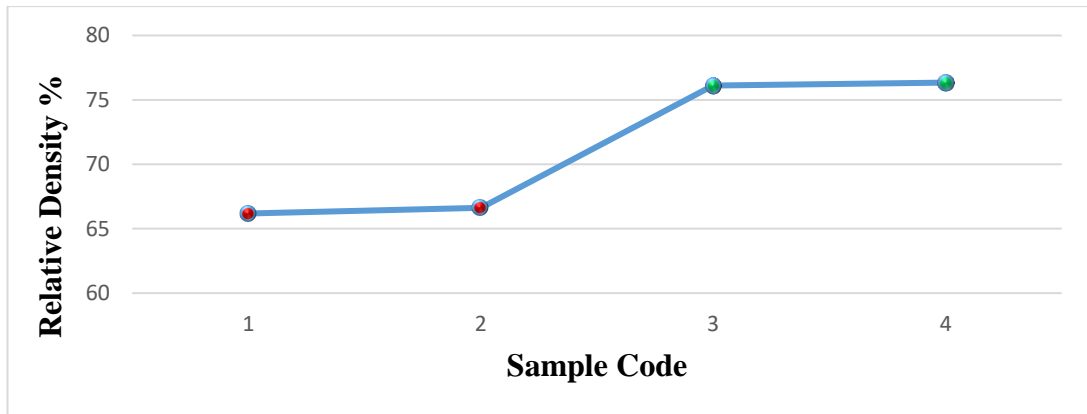


Figure 3.7: Effect of sintering atmosphere on the density of parts with 15-45  $\mu\text{m}$  powders. Samples 1 & 2 correspond to 95/5% N<sub>2</sub>/H<sub>2</sub> sintering, and samples 3 & 4 correspond to 100% H<sub>2</sub> sintering

### 3.3.4 Effects of Sintering Time on Density

In Figure 3.8, the 15-45  $\mu\text{m}$  low oxygen copper cubes sintered with the sintering regime, which was debinding at 450 °C for 30 minutes, oxidation-reduction at 700 °C for 1 hour and sintering at 1070 °C for 4 hours with 5°C/min. Prolonged sintering time yields higher relative density when comparing with the 2 hours of sintering.

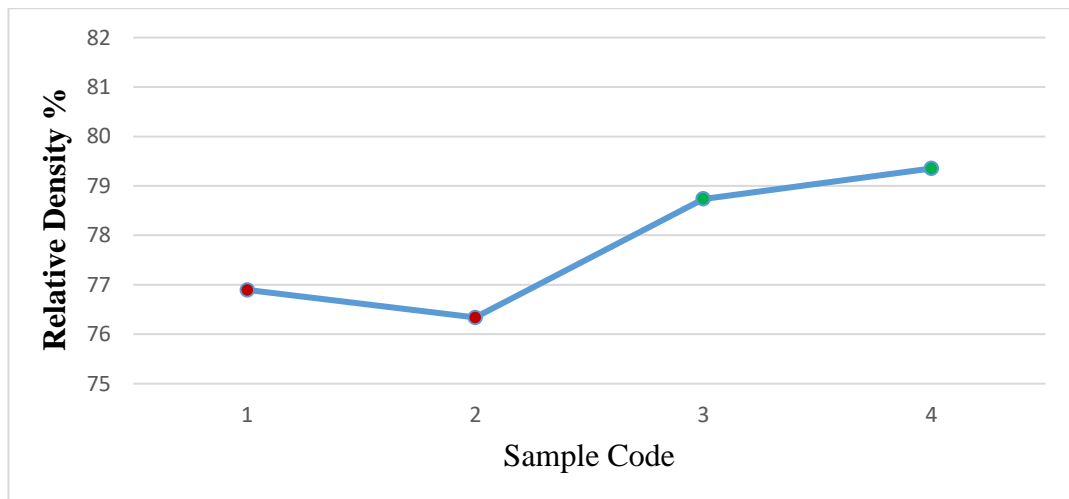


Figure 3.8: Effects of sintering time. Sample 1 & 2 correspond to sintering at 1070 °C 2 hours and Sample 3 & 4 correspond to sintering at 1070 °C 4 hours

### 3.3.5 Effects of Reduction Process Temperature on Density

As it seen in Figure 3.9, the 15-45  $\mu\text{m}$  low oxygen copper cubes sintered under 95/5% nitrogen/hydrogen with the sintering ramp, which was debinding at 450 °C for 30 minutes, oxidation-reduction at 900 °C for 1 hour and sintering at 1070 °C for 4 hours with 5°C/min. . Increase in oxide reduction process temperature yields small increase on relative density (79%  $\rightarrow$  81%) when comparing with the sintering atmosphere, sintering time.

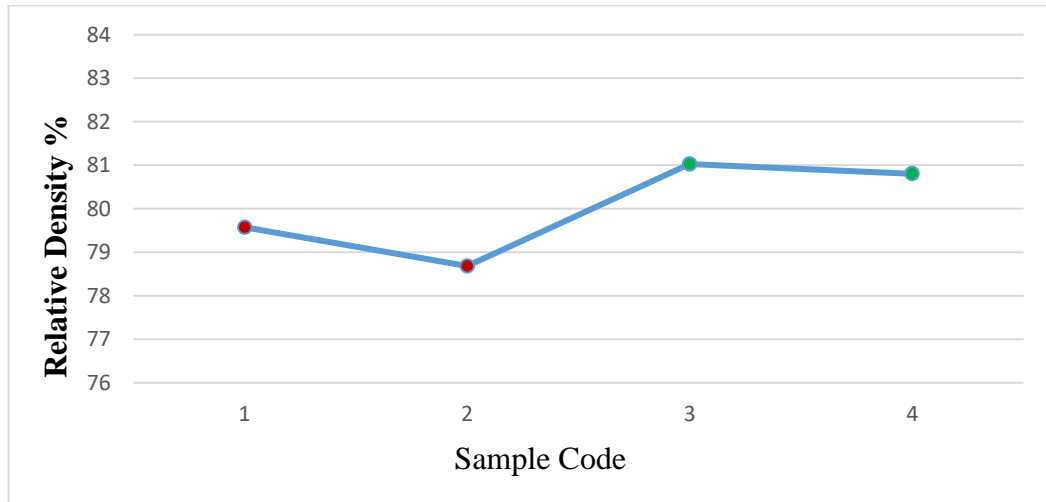


Figure 3.9: Effects of oxide reduction temperature. Sample 1 & 2 sintered with oxidation-reduction temperature at 700 °C and sample 3 & 4 sintered with oxidation reduction at 900 °C

### 3.4 Density, Porosity and Shrinkage Results

The high and low oxygen content 15-45  $\mu\text{m}$ , and low oxygen content 10-63 copper powders were printed in binder jetting at Istanbul Technical University EKAM with the parameters as determined in Section 3.3.2. After that the samples have been cured to obtain green parts as shown in Figure 3.10 (a).



(a)

(b)



(c)

Figure 3.10: (a) High oxygen content 15-45  $\mu\text{m}$  green parts printed with binder jetting, (b) sintered LO-10-63 cubes, and (c) sintered LO-15-45 parts

The cured cubes were sintered using the sintering ramp, which contains debinding at 450 °C for 30 minutes, oxidation-reduction at 900 °C for 1 hour and sintering at 1070 °C for 4 hours with 5°C/min heating rate under 100% hydrogen atmosphere. The results of green density, relative density and shrinkage were compared. Moreover, optic microscope and image j results are showed in Table 3.7. The highest green density was resulted in LO 10-63 samples, followed by LO 15-45. Parallel to green density, LO 10-63 sample shows the highest sinter density which is equal to 82,4 % of relative density.

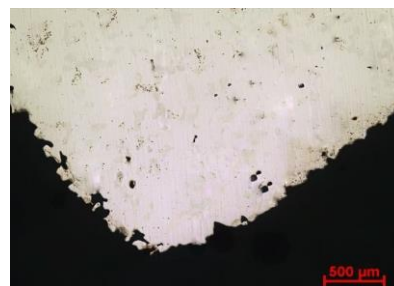
Table 3.7: Comparison of green, sintered and relative density, porosity and shrinkage results.

Sample code	Green Density (g/cm <sup>3</sup> )	Sintered Bulk Density (g/cm <sup>3</sup> )	Relative Density (%)	Porosity (Image analysis) (%)	Shrinkage (%)
LO-15-45	4,54	7,38	81,0	11,6	40,3 ±0,9
HO-15-45	4,38	7,26	77,9	13,8	34,8 ±1,2
LO-10-63	4,67	6,98	82,4	23,4	28,8 ±3,5

### 3.5 Optical Microscopy

In Figure 3.11 (a), (b), (c), and (d) when the microstructure images of L-O 15-45 samples are examined, it is observed that the porosities are homogeneously distributed. It can be seen that the amount of porosity is similar to each other both in the corners and in the inner regions. On the other hand, in the H-O 15-45 samples, the porosities are inhomogeneously distributed and the amount of porosity shows differences in the corners and inner regions as seen in Figure 3.11 (e), (f), (g), and (h).

In Figure 3.11 (i), (j), (k), and (l) the 1-O 10-63 samples are examined, it is seen that the porosities are homogeneously distributed, but it can be seen that the porosity sizes are quite large compared to the other samples.



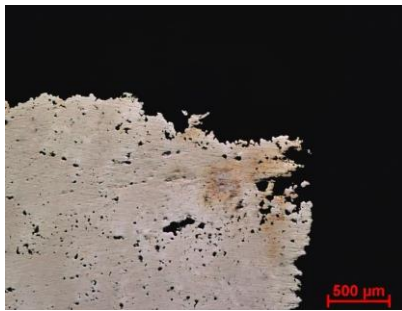
(a)



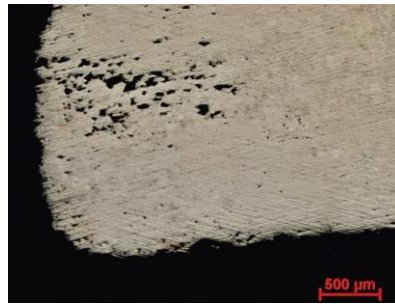
(b)



(c)



(d)



(e)



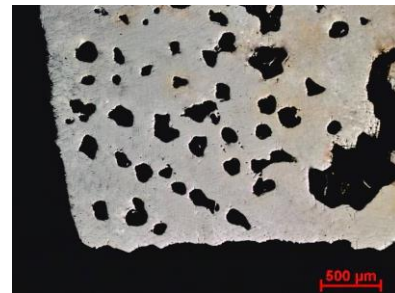
(f)



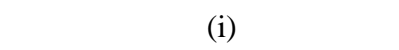
(g)



(h)



(i)



(j)



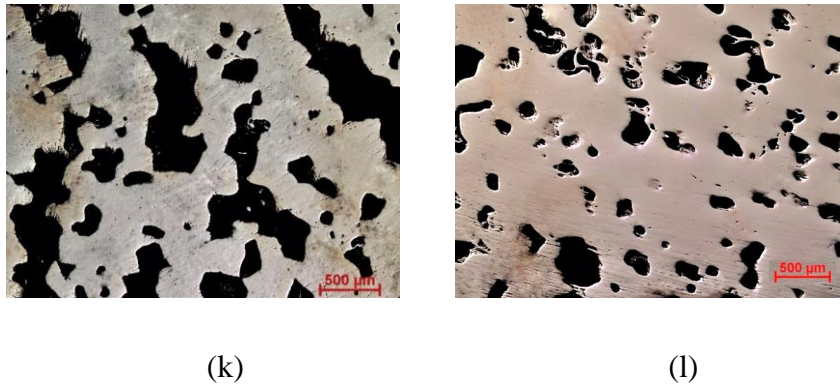


Figure 3.11: Optical microscope images of (a,b,c,d) LO-15-45, (e,f,g,h) HO-15-45, and (i,j,k,l) LO-10-63 parts

In Figure 3.12, image analysis was done using the image j program to determine the porosity ratios of the images obtained with the optical microscope. While H0-10-63 fragments have the highest relative density, it can be observed that it has the highest porosity by image analysis. Considering the other samples, L-O-15-45 has the lowest porosity rate and in H-O-15-45 samples also shows similar results.

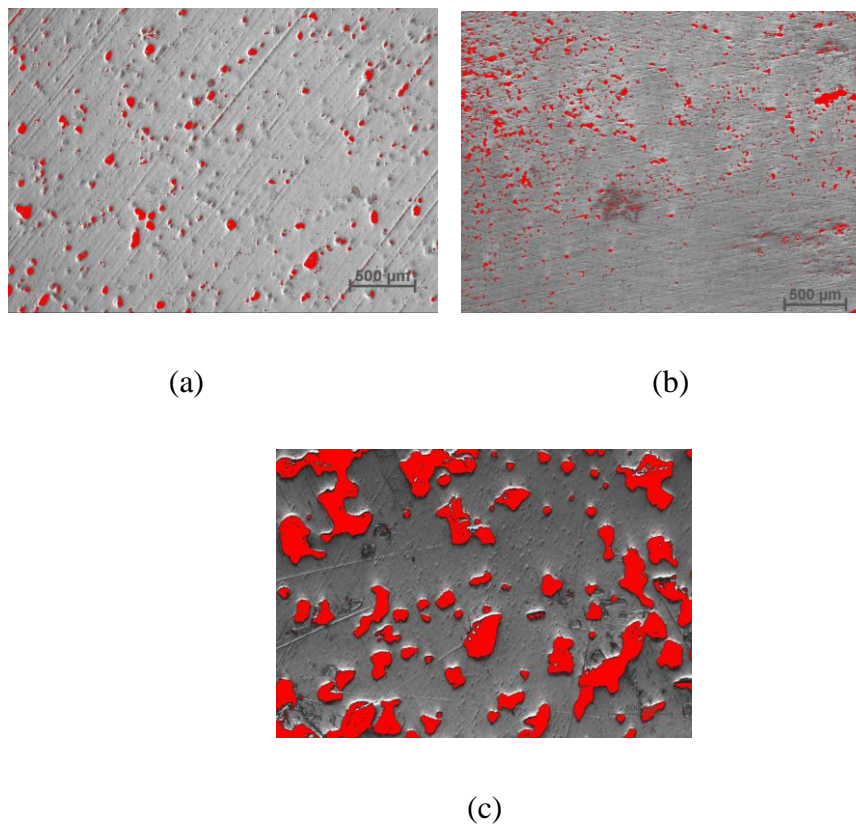


Figure 3.12: (a) High oxygen content 15-45 μm green parts printed with binder jetting, (b) sintered LO-15-45 parts sintered, and (c) LO-10-63 cubes

### 3.6 Surface Roughness Measurements

The surface roughness of all cube and circle samples gave results as seen in the Table 3.8. The lowest surface roughness is seen in the H-O-15-45 cube, while the highest value is seen in the L-O-10-63 cube. However, when circular samples are examined, L-O-15-45 and H-O-15-45 show similar surface roughness, and L-O-10-63 samples show the highest surface roughness in both cubes and circles.

Table 3.8: Comparison of surface roughness values of the samples

Sample code/shape	R <sub>a</sub>	R <sub>q</sub>	R <sub>t</sub>
LO-15-45/cube	14,4	18,7	99,1
HO-15-45/cube	8,6	10,9	62,2
LO-10-63/cube	17,8	24,4	131,8
LO-15-45/circle	10,4	14,5	80,6
HO-15-45/circle	10,8	15,6	82,4
LO-10-63/circle	15,9	21,1	119,8

### 3.7 Electrical Properties

As can be seen in the Table 3.9, L-O-10-63 samples showed the lowest electrical resistivity and conductivity. L-O-15-45 has the highest electrical resistivity and conductivity values. H-O-15-45 samples shows similar results with L-O-15-45.

Table 3.9: Electrical conductivity test results

Sample code	Resistivity (ohm/m)	Electrical Conductivity (m/ohm)
LO-15-45 cube	2405,10	4,15
HO-15-45 cube	3264,69	3,03
LO-10-63 cube	3576,4	2,8

When the density results that have a great effect on the electrical properties are examined, the highest density was obtained in the samples produced with LO-15-45 pure copper powders, as seen in the results of bulk density, optical microscope and image analysis. The electrical conductivity results show that the electrical properties increase as the sintering temperature increases, due to the decrease in porosities and with the decrease in the average particle size distribution of pure copper powders. This is due to the nature of a porosity that inhibits the electron transfer.

### 3.8 Tensile Tests Results

As can be seen in the Table 3.10, the L-O-15-45 samples shows the highest yield and tensile strength values. Also, L-O-15-45 samples show highest ductility. On the other hand, L-O-10-63 samples show the lowest tensile strength and ductility. When oxygen levels are compared, L-O-15-45 samples show better tensile results.

Table 3.10: Tensile test results

Samples	Yield Strength (MPa)	Ultimate Strength (MPa)	Strain (%)
L-O-15-45	25,7 ±3,6	95,5 ±9	14,3 ±2,1
H-O-15-45	20,5 ±1,8	76,0 ±45,3	10,5 ±7,8
L-O-10-63	21,1 ±0,9	62,5 ±33,6	10,0 ±6,3

Yun Bai et al. carried out sintering studies by mixing pure copper powders of different particle sizes in different proportions, obtaining different bimodal particle size distribution and pressing with binder jetting additive manufacturing method. In their results, they obtained the highest density when they used the smallest median size which is 15  $\mu\text{m}$ . In opposition to these results, when the study made with L-O 15-45 and L-O 10-63 micron pure copper powders are examined, the average particle sizes of the powders with this particle size distribution are 25 micron and 33 micron, and the Archimedes density results are found as 82.4 % and 81%, respectively. However, bulk density results are similar, and increase with decreasing of the median particle size. The reason that Archimedes density gives the opposite of the bulk density is due to the fact that the surface quality of the cube produced with the powder with 10-63 particle size distribution is better and absorbs the silicon oil less, and when the image analysis and bulk analysis results are examined, it is easily understood that the 10-63 particle size distribution gives a lower density.

Hadi Miyanaji et al. investigated the effect of fine pure copper powders on the parts produced in binder jetting. In their results, they observed that when the average particle size increased, there was a decrease in the ultimate tensile strength results. When it is compared with this study, the samples produced with pure copper powders with a particle size distribution of L-O 15-45  $\mu\text{m}$  have obtained approximately 51% higher ultimate tensile strength (95,5 MPa) than the samples produced with L-O 10-63  $\mu\text{m}$  pure copper (62,5 MPa).

Ashwath Yegyan Kumara et al. investigated the effect of process-induced porosities on mechanical, electrical and thermal properties by producing various characterization samples in binder spraying using pure copper powders. They used four wire measurement apparatus for electrical conductivity analysis and calculated electrical conductivity using the Wiedemann-Franz Law. It has been observed that the electrical conductivity increases when the average particle size distribution decreases and the best results are obtained with bimodal powders. Compared to the results of this study, 4 point measurement was used instead of four wire measurement and similar results observed that the electrical conductivity increased when the 15-45  $\mu\text{m}$  particle size distribution is used instead of 10-63  $\mu\text{m}$  particle size distribution.

# Chapter 4

## Conclusions

Conclusions of benchtops test results can be summarize below;

- 1) As a benchtop test result, it was found that the mixture with 5% binder and 95% copper powder has the most suitable viscosity for casting into the bar and most suitable mold was the silicone mold, since the samples easily have been took off from the bars.
- 2) It was observed that the benchtop samples cured at 200 °C for 2 hours were oxidized under open atmosphere. For this reason, it was seen that a protective atmosphere should be used during curing. Oxidation did not occur in the samples cured under argon gas.
- 3) It was observed that the benchtop test specimens had lower density, when comparing the sintered benchtop test specimens with the binder jetting specimens. Therefore, it was concluded that the benchtop test method is a suitable method to test the compatibility of binder and powder, curing behavior before printing with binder jetting, but it is not sufficient to test the properties after sintering.

Conclusions of binder jetting results are listed below;

- 1) When samples were produced using the binder jetting additive manufacturing method with copper powders with 2 different particle size distributions (15-45 and 10-63) and 2 different oxygen levels, and their physical and electrical properties were compared. Since 15-45 samples with low oxygen show more stable results in general, it has been observed that it is more advantageous than 10-63 and high oxygen copper powders.
- 2) Cube samples produced with <45 μm low oxygen copper powders were sintered under 95/5% nitrogen/hydrogen atmosphere at different temperatures of 1040 °C, 1050

°C and 1070 °C, and their relative densities were measured. The highest relative density was obtained at the sintering temperature of 1070 °C.

3) In order to examine the effect of the binder ratio, cube samples were produced using low and medium amounts of binder. It was observed that the relative densities of the cubes with a low ratio of binder were better.

4) As another study, the effect of sintering atmosphere was investigated. Samples sintered under 100% H<sub>2</sub> atmosphere gave approximately 15% higher relative density results than samples sintered in 95/5% N<sub>2</sub>/H<sub>2</sub> atmosphere.

5) When the effect of sintering time on relative density was examined, samples sintered for 4 hours resulted in higher relative density than samples sintered for 2 hours. Also, results showed that the effect of oxide reduction temperature on relative density was not drastic; however, a small improvement in relative density was observed with oxide reduction performed at 900 °C.

6) When the results of the samples produced with LO-15-45 and HO-15-45 powders in the same sintering regime, the samples with higher oxygen resulted lower relative density. However, LO-10-63 samples resulted in the highest relative density compared to LO-15-45 and HO-15-45 samples. As a result of the subsequent microstructure analysis, it was observed that the largest porosity size and ratio was in the LO-10-63 samples. Surface roughness analysis was performed to find out the reason for the high relative densities of the LO-10-63 samples, and considering the results, it was understood that the relative density values of the LO-10-63 samples were high because the surface roughness values of the LO-10-63 samples were high.

7) As the electrical properties were compared, the LO-15-45 samples result the best electrical conductivity due to both low porosity and low oxygen level.

8) Finally, the tensile test results were examined, the worst results were showed in the HO-10-63 samples. This is due to the high pore size and porosity level of HO-10-63 samples. On the other hand, the results of LO-15-45 and HO-15-45 samples are examined, and similar results are obtained, but LO-15-45 gives better results.

# References

- [1] Koike M, Greer P, Owen K *et al.* Evaluation of titanium alloys fabricated using rapid prototyping technologies-electron beam melting and laser beam melting. *Materials* 2011; 4: 1776–1792.
- [2] Tran TQ, Chinnappan A, Lee JKY *et al.* 3D printing of highly pure copper. *Metals* 9 2019.
- [3] Cozmei C, Caloian F. Additive Manufacturing Flickering at the Beginning of Existence. *Procedia Economics and Finance* 2012; 3: 457–462.
- [4] Ngo TD, Kashani A, Imbalzano G, Nguyen KTQ, Hui D. Additive manufacturing (3D printing): A review of materials, methods, applications and challenges. *Composites Part B: Engineering* 143 2018 172–196.
- [5] Harun WSW, Kamariah MSIN, Muhamad N, Ghani SAC, Ahmad F, Mohamed Z. A review of powder additive manufacturing processes for metallic biomaterials. *Powder Technology* 327 2018 128–151.
- [6] Asadollahiyazdi E, Gardan J, Lafon P. Integrated Design in Additive Manufacturing Based on Design for Manufacturing Design for Additive Manufacturing (DFAM) View project. 2016.
- [7] Thompson SM, Bian L, Shamsaei N, Yadollahi A. An overview of Direct Laser Deposition for additive manufacturing; Part I: Transport phenomena, modeling and diagnostics. *Additive Manufacturing* 8 2015 36–62.
- [8] Svetlizky D, Das M, Zheng B *et al.* Directed energy deposition (DED) additive manufacturing: Physical characteristics, defects, challenges and applications. *Materials Today* 49 2021 271–295.

- [9] Leary M. Powder bed fusion. In: Design for Additive Manufacturing. Elsevier, 2020: 295–319.
- [10] Sun S, Brandt M, Easton M. Powder bed fusion processes. In: Laser Additive Manufacturing. Elsevier, 2017: 55–77.
- [11] Vock S, Klöden B, Kirchner · Alexander, Weißgärber T, Kieback · Bernd. Powders for powder bed fusion: a review. 2019; 4: 383–397.
- [12] Kruth JP, Wang X, Laoui T, Froyen L. Lasers and materials in selective laser sintering. .
- [13] Mercelis P, Kruth JP. Residual stresses in selective laser sintering and selective laser melting. Rapid Prototyping Journal 2006; 12: 254–265.
- [14] Yap CY, Chua CK, Dong ZL *et al.* Review of selective laser melting: Materials and applications. Applied Physics Reviews 2 2015.
- [15] Shipley H, McDonnell D, Culleton M *et al.* Optimisation of process parameters to address fundamental challenges during selective laser melting of Ti-6Al-4V: A review. International Journal of Machine Tools and Manufacture 128 2018 1–20.
- [16] Galati M, Iuliano L. A literature review of powder-based electron beam melting focusing on numerical simulations. Additive Manufacturing 2018; 19: 1–20.
- [17] Negi S, Nambolan AA, Kapil S *et al.* Review on electron beam based additive manufacturing. Rapid Prototyping Journal 26 2020 485–498.
- [18] Körner C. Additive manufacturing of metallic components by selective electron beam melting — a review. International Materials Reviews 2016; 61: 361–377.
- [19] Gong X, Anderson T, Chou K. Review on powder-based electron beam additive manufacturing technology. Manufacturing Review 2014; 1: 2.
- [20] Zhang L, Liu Y, Li S, Hao Y. Additive Manufacturing of Titanium Alloys by Electron Beam Melting: A Review. Advanced Engineering Materials 2018; 20: 1700842.

- [21] Koike M, Greer P, Owen K *et al.* Evaluation of Titanium Alloys Fabricated Using Rapid Prototyping Technologies—Electron Beam Melting and Laser Beam Melting. *Materials* 2011; 4: 1776–1792.
- [22] Gibson I, Rosen DW, Stucker B. Sheet Lamination Processes. In: *Additive Manufacturing Technologies*. Springer US, 2010: 223–252.
- [23] Mekonnen BG, Bright G, Walker A. A study on state of the art technology of laminated object manufacturing (Lom). *Lecture Notes in Mechanical Engineering* 2016; 207–216.
- [24] Weisensel L, Travitzky N, Sieber H, Greil P. Laminated Object Manufacturing (LOM) of SiSiC composites. *Advanced Engineering Materials* 2004; 6: 899–903.
- [25] Braconnier DJ, Jensen RE, Peterson AM. Processing parameter correlations in material extrusion additive manufacturing. *Additive Manufacturing* 2020; 31.
- [26] Danut Mazurchevici A, Nedelcu D, Popa R. Additive manufacturing of composite materials by FDM technology: A review. 2020.
- [27] Park SI, Rosen DW, Choi S kyum, Duty CE. Effective mechanical properties of lattice material fabricated by material extrusion additive manufacturing. *Additive Manufacturing* 2014; 1: 12–23.
- [28] Dilag J, Chen T, Li S, Bateman SA. Design and direct additive manufacturing of three-dimensional surface micro-structures using material jetting technologies. *Additive Manufacturing* 2019; 27: 167–174.
- [29] Gülcan O, Günaydın K, Tamer A. The state of the art of material jetting—a critical review. *Polymers* 13 2021.
- [30] Andreu A, Su PC, Kim JH *et al.* 4D printing materials for vat photopolymerization. *Additive Manufacturing* 44 2021.
- [31] Nohut S, Schwentenwein M. Vat Photopolymerization Additive Manufacturing of Functionally Graded Materials: A Review. *Journal of Manufacturing and Materials Processing* 6 2022.

- [32] Gibson I, Rosen D, Stucker B, Khorasani M. Additive Manufacturing Technologies. .
- [33] Mostafaei A, Elliott AM, Barnes JE *et al.* Binder jet 3D printing—Process parameters, materials, properties, modeling, and challenges. *Progress in Materials Science* 119 2021.
- [34] Gaytan SM, Cadena MA, Karim H *et al.* Fabrication of barium titanate by binder jetting additive manufacturing technology. *Ceramics International* 2015; 41: 6610–6619.
- [35] Myers K, Paterson A, Iizuka T, Klein A. The Effect of Print Speed on Surface Roughness and Density Uniformity of Parts Produced Using Binder Jet 3D Printing. .
- [36] Miyanaji H, Rahman KM, Da M, Williams CB. Effect of fine powder particles on quality of binder jetting parts. *Additive Manufacturing* 2020; 36.
- [37] Gokuldoss PK, Kolla S, Eckert J. Additive manufacturing processes: Selective laser melting, electron beam melting and binder jetting-selection guidelines. *Materials* 10 2017.
- [38] Gobbin F, Elsayed H, Italiano A, Adrien J, Colombo P, Maire E. Large scale additive manufacturing of artificial stone components using binder jetting and their X-ray microtomography investigations. *Open Ceramics* 2021; 7.
- [39] Atapour M, Wang X, Persson M, Odnevall Wallinder I, Hedberg YS. Corrosion of Binder Jetting Additively Manufactured 316L Stainless Steel of Different Surface Finish. *Journal of The Electrochemical Society* 2020; 167: 131503.
- [40] Garzón EO, Alves JL, Neto RJ. Post-process influence of infiltration on binder jetting technology. *Advanced Structured Materials*, Springer Verlag 2017, 233–255.
- [41] Miyanaji H, Momenzadeh N, Yang L. Effect of powder characteristics on parts fabricated via binder jetting process. *Rapid Prototyping Journal* 2019; 25: 332–342.

- [42] Kassym K, Perveen A. Atomization processes of metal powders for 3D printing. *Materials Today: Proceedings*, Elsevier Ltd 2019, 1727–1733.
- [43] Lagutkin S, Achelis L, Sheikhaliev S, Uhlenwinkel V, Srivastava V. Atomization process for metal powder. *Materials Science and Engineering A* 2004; 383: 1–6.
- [44] Zheng B, Lin Y, Zhou Y, Lavernia EJ. Gas atomization of amorphous aluminum powder: Part II. experimental investigation. *Metallurgical and Materials Transactions B: Process Metallurgy and Materials Processing Science* 2009; 40: 995–1004.
- [45] Atomization. *Encyclopedia of Materials: Science and Technology (Second Edition)*. 2001, Pages 387-392
- [46] Popov V v., Grilli ML, Koptug A *et al.* Powder bed fusion additive manufacturing using critical raw materials: A review. *Materials* 2021; 14: 1–37.
- [47] Lv X, Ye F, Cheng L, Fan S, Liu Y. Binder jetting of ceramics: Powders, binders, printing parameters, equipment, and post-treatment. *Ceramics International* 45 2019 12609–12624.
- [48] Chen Q, Juste E, Lasgorceix M, Petit F, Leriche A. Binder jetting process with ceramic powders: Influence of powder properties and printing parameters. *Open Ceramics* 2022; 9.
- [49] Strondl A, Lyckfeldt O, Brodin H, Ackelid U. Characterization and Control of Powder Properties for Additive Manufacturing. *JOM* 2015; 67: 549–554.
- [50] Mirzababaei S, Pasebani S. A review on binder jet additive manufacturing of 316L stainless steel. *Journal of Manufacturing and Materials Processing* 3 2019.
- [51] Lores A, Azurmendi N, Agote I, Zuza E. A review on recent developments in binder jetting metal additive manufacturing: materials and process characteristics. *Powder Metallurgy* 62 2019 267–296.
- [52] Du W, Ren X, Ma C, Pei Z. BINDER JETTING ADDITIVE MANUFACTURING OF CERAMICS: A LITERATURE REVIEW. 2017.

- [53] Johnson JL, Tan LK, Bollina R, Suri P, German RM. Evaluation of copper powders for processing heat sinks by metal injection moulding. *Powder Metallurgy* 2005; 48: 123–128.
- [54] Tasić ŽZ, Petrović Mihajlović MB, Radovanović MB, Antonijević MM. New trends in corrosion protection of copper. *Chemical Papers* 73 2019 2103–2132.
- [55] Islak S, Kir D, Buytoz S. Effect of sintering temperature on electrical and microstructure properties of hot pressed Cu-TiC composites. *Science of Sintering* 2014; 46: 15–21.
- [56] Jiang Q, Zhang P, Yu Z *et al.* A review on additive manufacturing of pure copper. *Coatings* 11 2021.
- [57] Bai Y, Williams CB. An exploration of binder jetting of copper. *Rapid Prototyping Journal* 2015; 21: 177–185.
- [58] Bai Y, Wagner G, Williams CB. Effect of Bimodal Powder Mixture on Powder Packing Density and Sintered Density in Binder Jetting of Metals. .
- [59] Kumar A, Bai Y, Eklund A, Williams CB. Effects of Hot Isostatic Pressing on Copper Parts Fabricated via Binder Jetting. *Procedia Manufacturing*, Elsevier B.V. 2017, 935–944.
- [60] Yegyan Kumar A, Wang J, Bai Y, Huxtable ST, Williams CB. Impacts of process-induced porosity on material properties of copper made by binder jetting additive manufacturing. *Materials and Design* 2019; 182.
- [61] Miyanaji H, Rahman KM, Da M, Williams CB. Effect of fine powder particles on quality of binder jetting parts. *Additive Manufacturing* 2020; 36.
- [62] Barthel B, Janas F, Wieland S. Powder condition and spreading parameter impact on green and sintered density in metal binder jetting. *Powder Metallurgy* 2021; 64: 378–386.
- [63] Do T, Kwon P, Shin CS. Process development toward full-density stainless steel parts with binder jetting printing. *International Journal of Machine Tools and Manufacture* 2017; 121: 50–60.

- [64] Ott J, Burghardt A, Britz D, Mücklich F. Influence of porosity and impurities on the thermal conductivity of pressure-less sintered Cu powder green bodies. *Powder Metallurgy* 2021; 64: 85–96.
- [65] Enrique PD, Mahmoodkhani Y, Marzbanrad E, Toyserkani E, Zhou NY. In situ formation of metal matrix composites using binder jet additive manufacturing (3D printing). *Materials Letters* 2018; 232: 179–182.
- [66] Li M, Huang J, Fang A, Mansoor B, Pei Z, Ma C. Binder jetting additive manufacturing of copper/diamond composites: An experimental study. *Journal of Manufacturing Processes* 2021; 70: 205–213.
- [67] Li M, Miao G, Moghadasi M, Pei Z, Ma C. Ceramic binder jetting additive manufacturing: Relationships among powder properties, feed region density, and powder bed density. *Ceramics International* 2021; 47: 25147–25151.
- [68] Bai Y Williams Alex O Aning Thomas E Diller Peizhen Lu Carlos T A Suchicital Xiaoyu Zheng C. Additive Manufacturing of Copper via Binder Jetting of Copper Nanoparticle Inks. 2018; 31.
- [69] <https://www.3dprintingmedia.network/digital-metal-to-offer-dm-cu-pure-copper-as-a-material-for-its-binder-jetting-system/>

# Appendices

# Appendix A

## Publications from the Thesis

### **Conference Papers**

1. “Particle Size Effects on Sintering of Binder Jetting Copper”. III. International Science and Innovation Congress to be held on 09-12 June 2022

# Curriculum Vitae

Name Surname : Cem Özateş  
E-mail (1) : Y190219003@ikcu.edu.tr  
E-mail (2) : cemozates@gmail.com

## Education:

2012–2018 Anadolu University, Dept. of Material Science and  
Engineering.

## Work Experience:

(2020 – ....) Sentes-BIR A.Ş